






The varved succession of Crawford Lake, Milton, Ontario, Canada as a candidate Global boundary Stratotype Section and Point for the Anthropocene series

The Anthropocene Review
2023, Vol. 10(1) 146–176
© The Author(s) 2023
Article reuse guidelines:
sagepub.com/journals-permissions
DOI: 10.1177/20530196221149281
journals.sagepub.com/home/anr



Francine MG McCarthy,¹  R. Timothy Patterson,²
Martin J Head,¹ Nicholas L Riddick,¹ Brian F Cumming,³
Paul B Hamilton,⁴ Michael FJ Pisaric,¹ A. Cale Gushulak,⁵ 
Peter R Leavitt,⁵  Krysten M Lafond,² Brendan Llew-Williams,¹
Matthew Marshall,² Autumn Heyde,¹ Paul M Pilkington,¹
Joshua Moraal,¹ Joseph I Boyce,⁶ Nawaf A Nasser,²
Carling Walsh,² Monica Garvie,³ Sarah Roberts,⁷ Neil L Rose,⁷
Andy B Cundy,⁸ Pawel Gaca,⁸ Andy Milton,⁸ Irka Hajdas,⁹ 
Carley A Crann,¹⁰ Arnoud Boom,¹¹ Sarah A Finkelstein,¹² John
H McAndrews¹² and other members of Team Crawford

Abstract

An annually laminated succession in Crawford Lake, Ontario, Canada is proposed for the Global boundary Stratotype Section and Point (GSSP) to define the Anthropocene as a series/epoch with a base dated at 1950 CE. Varve couplets of organic matter capped by calcite precipitated each summer in alkaline surface waters reflect environmental change at global to local scales. Spheroidal carbonaceous particles and nitrogen isotopes record an increase in fossil fuel combustion in the early 1950s, coinciding with early fallout from nuclear and thermonuclear testing – ²³⁹⁺²⁴⁰Pu and ¹⁴C:¹²C, the latter more than compensating for the effects of old carbon in this dolomitic basin. Rapid industrial expansion in the North American Great Lakes region led to enhanced leaching of terrigenous elements by acid precipitation during the Great Acceleration, and calcite precipitation was reduced, producing thin calcite laminae around the GSSP that is marked by a sharp decline in elm pollen (Dutch Elm disease). The lack of bioturbation in well-oxygenated bottom waters, supported by the absence of fossil pigments from obligately anaerobic purple sulfur bacteria, is attributed to elevated salinities and high alkalinity below the chemocline. This

¹Brock University, Canada

²Carleton University, Canada

³Queen's University, Canada

⁴Canadian Museum of Nature, Canada

⁵University of Regina, Canada

⁶McMaster University, Canada

⁷University College London, UK

⁸University of Southampton, UK

⁹ETH Zürich, Switzerland

¹⁰University of Ottawa, Canada

¹¹University of Leicester, UK

¹²University of Toronto, Canada

Corresponding author:

Francine MG McCarthy, Department of Earth Sciences,
Brock University, 1812 Sir Isaac Brock Way, St.
Catharines, Ontario L2S 3A1, Canada.
Email: fmccarthy@brocku.ca

aerobic depositional environment, highly unusual in a meromictic lake, inhibits the mobilization of Pu, the proposed primary stratigraphic guide for the Anthropocene.

Keywords

acid precipitation, combustion, Dutch Elm disease, Great Acceleration, fossil plankton, μ XRF, radionuclides, SCPs, stable isotopes, varves

Introduction

Annual resolution of local, regional, and global events recorded by a variety of proxies is possible in laminated (varved) sediments in the deep basin of Crawford Lake, Ontario, Canada. The sediments have received considerable attention since the discovery of *Zea* (maize/corn) pollen in varves deposited centuries before European colonization (Boyko, 1973; Boyko-Diakonow, 1979; McAndrews and Boyko-Diakonow, 1989; see McCarthy, 2022). Most early studies focused on the record of Indigenous agricultural settlement, colonial land clearing and logging, and the resulting ecosystem changes (Byrne and Finlayson, 1998; Ekdahl et al., 2004, 2007; Finlayson et al., 1973; Krueger and McCarthy, 2016; McAndrews and Turton, 2007, 2010; Turton and McAndrews, 2006; Figure 1). Subsequent analysis of siliceous microfossil assemblages and pigments at relatively high resolution through the 20th century in gravity cores revealed substantial changes in algal communities around 1954 CE (Rybak and Dickman, 1988; Rybak et al., 1987; Supplemental Figure S1). The results of these previous studies suggested that the varved succession might be examined at higher

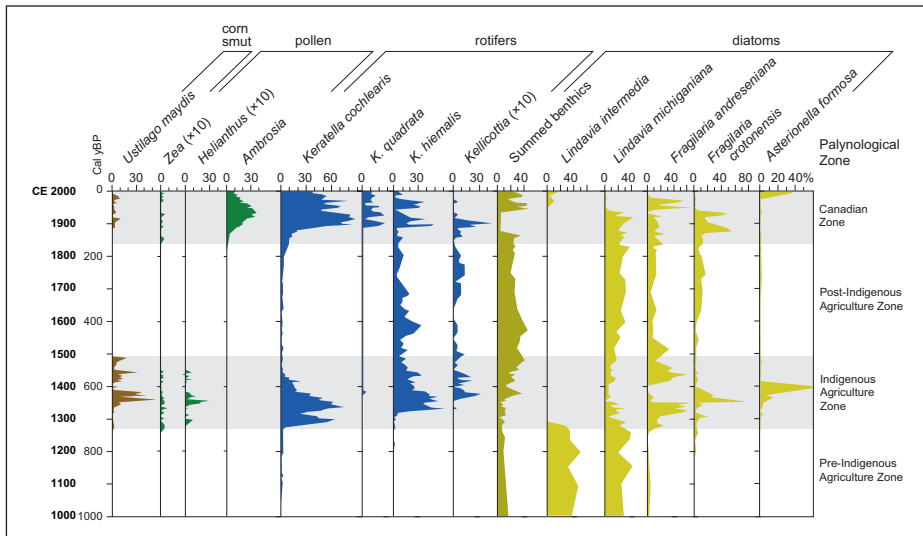


Figure 1. Diatoms and the rotifers that consume them were abundant in Crawford Lake during intervals of human impact (shading), recorded by the pollen of cultigens (e.g., *Zea* – maize and *Helianthus* – sunflower) and spores of their pathogens (e.g., *Ustilago maydis* – corn smut), and nonarbooreal pollen (e.g., ragweed – *Ambrosia*). $\times 10$ = ten times exaggeration of rare but significant elements in palynological preparations. Palynomorph data from Turton and McAndrews (2006), diatom data modified from Ekdahl et al. (2004) with updated taxonomic nomenclature – *Lindavia intermedia* = *Cyclotella bodanica lemanica* and *Lindavia michiganiana* = *Cyclotella michiganiana*. Diatoms identified as *Synedra nana* by Ekdahl et al. (2004) are likely to have been various large *Fragilaria* spp., including the common *Fragilaria andreseniana* (compare Figure 16). Reproduced in color in online version.

resolution as a potential candidate for an Anthropocene Global boundary Stratotype Section and Point (GSSP) which would align with the mid-20th century, when extraordinary human energy consumption and productivity transformed the Earth System state (Syvitski et al., 2020).

Crawford Lake is in the highly industrialized Lower Great Lakes region of North America, NNW of Hamilton, Ontario (Supplemental Figure S2), and readily accessible within 50 km of two international airports. Conservation Halton purchased what is now the Crawford Lake Conservation Area in 1969 and archeological excavations found evidence of at least two intervals of Indigenous agricultural settlement dating to the 14th and 15th centuries CE (Finlayson, 1998). This 94-ha conservation area on the Niagara Escarpment UNESCO Biosphere Reserve includes reconstructed longhouses and an interpretive boardwalk around the lake. Evidence of earlier localized anthropogenic impacts contrasts with the mid-20th century impacts and associated global perturbations that mark the onset of the proposed Anthropocene series/epoch. The preparatory activities of the Anthropocene Working Group, including events leading to the submission of GSSP proposals and the binding decision that the base of the Anthropocene should align with stratigraphic signals dating to the mid-20th century, are detailed in the introductory article to this special issue (Waters et al., 2023).

Materials and methods

Geographic setting of core sites

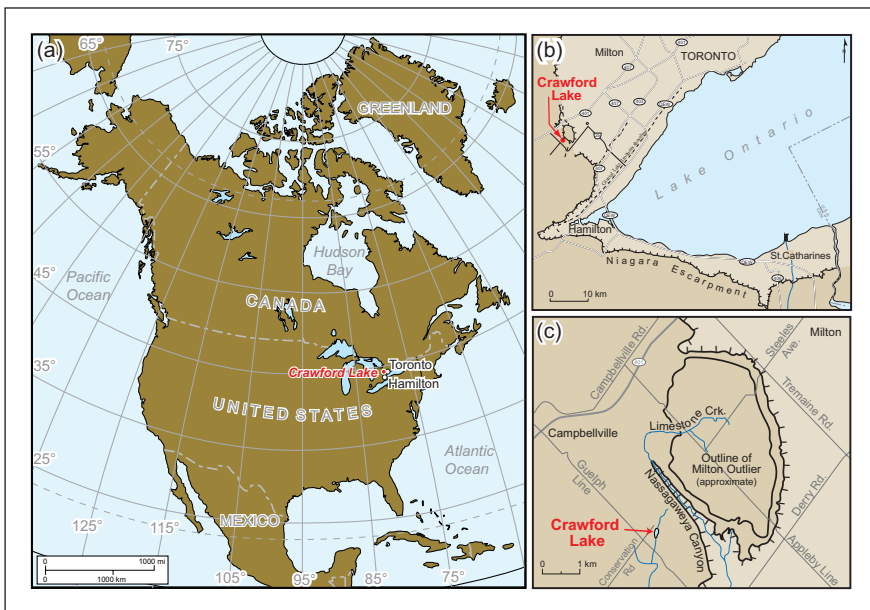


Figure 2. (a) Crawford Lake is in the Lower Great Lakes region of North America. (b) Location of the study site relative to the Niagara Escarpment and Milton Outlier (darker brown highlighting higher elevation), northeast of the industrial city of Hamilton. (c) Groundwater infiltrates hydraulically conductive units in the Silurian bedrock that transect the karstic basin of Crawford Lake at Nassagaweya Canyon (see Supplemental Figure S3). Reproduced in color in online version.

Crawford Lake (43.468658° N, 79.948726° W) is in the township of Milton, occupying a sinkhole dissolved in dolomitic limestones of the Silurian Lockport Group (Figure 2 and Supplemental Figure S3). Soil cover is thin and discontinuous except in the northwest of its ~91 ha catchment where arable soils formed on thick Wentworth Till (Karrow, 1987). Eastern white cedar (*Thuja occidentalis*) dominates the mixed forest, and common decay-resistant stumps of white pine (*Pinus strobus*) around the lake are evidence of logging in the mid- to late 19th century. The climate is humid continental, with warm summers and cold winters (mean July and January temperature 20.6°C and -6°C) and mean annual precipitation of 973 mm (https://climat.meteo.gc.ca/climate_normals/index_e.html).

This small (2.4ha), deep (Z_{max} . 24m) lake is meromictic, and studies of the water column have demonstrated that laminated sediments below the chemocline are varves, with calcite precipitated in summer capping organic matter accrued during fall turnover (Dickman, 1979, 1985). The depth-to-surface area ratio prevents mixing of the water column ($Z_r \sim 13.73$, much higher than the threshold of $Z_r > 2$ for meromixis according to Hutchinson, 1957), where Z_m =maximum depth and A =surface area:

$$Z_r = \frac{(50 \times Z_m \times \sqrt{\pi})}{(\sqrt{A})}$$

The mixolimnion represents the uppermost 15.5 m of the water column, comprises over 90% of the ~293,000 m³ lake volume, and does not mix with the underlying monimolimnion. A strong chemical density gradient reinforces a separation of waters below the chemocline (Figure 3) where the chemistry closely resembles that reported by Priebe (2019) for major aquifers in the Gasport Formation (Supplemental Figures S3 and S4). Input from the overlying Goat Island Formation to the mixolimnion is diluted by surface runoff, inflow from a single inlet stream, and direct precipitation. Crawford Lake is hydrologically open, with outflow ultimately entering Lake Ontario. Groundwater forms a significant component of Crawford Lake's water budget, transporting high concentrations of calcium bicarbonate into the karstic basin (Llew-Williams, 2022), and minimizing fluctuations in water level (~278m asl). Calcite precipitates in the upper 6m of Crawford Lake when water

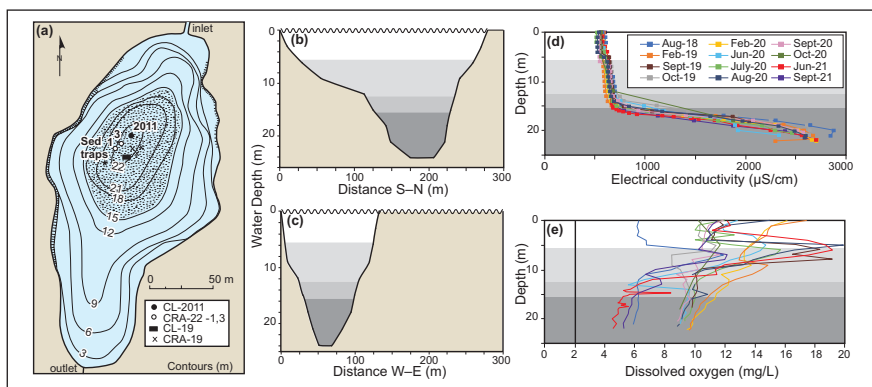


Figure 3. Bathymetry (from Boyko, 1973) and physical limnology of Crawford Lake. (a) The 15m isobath identifies the area below which seasonally laminated sediments accumulate and cross-sections (b, c) illustrate the small volume of the monimolimnion (darkest shading; see Figure S4 for water mass key). Measured physicochemical variables demarcate the water column zonation, with a permanent chemocline (~15.5 m) isolating the dense, electrically conductive monimolimnion (d) from the overlying mixolimnion. (e) Dissolved oxygen concentrations were highest in the metalimnion (lightest grey) but always exceeded the 2mg/L threshold for hypoxia in freshwater ecosystems (vertical line). Modified from Llew-Williams (2022). Reproduced in color in online version.

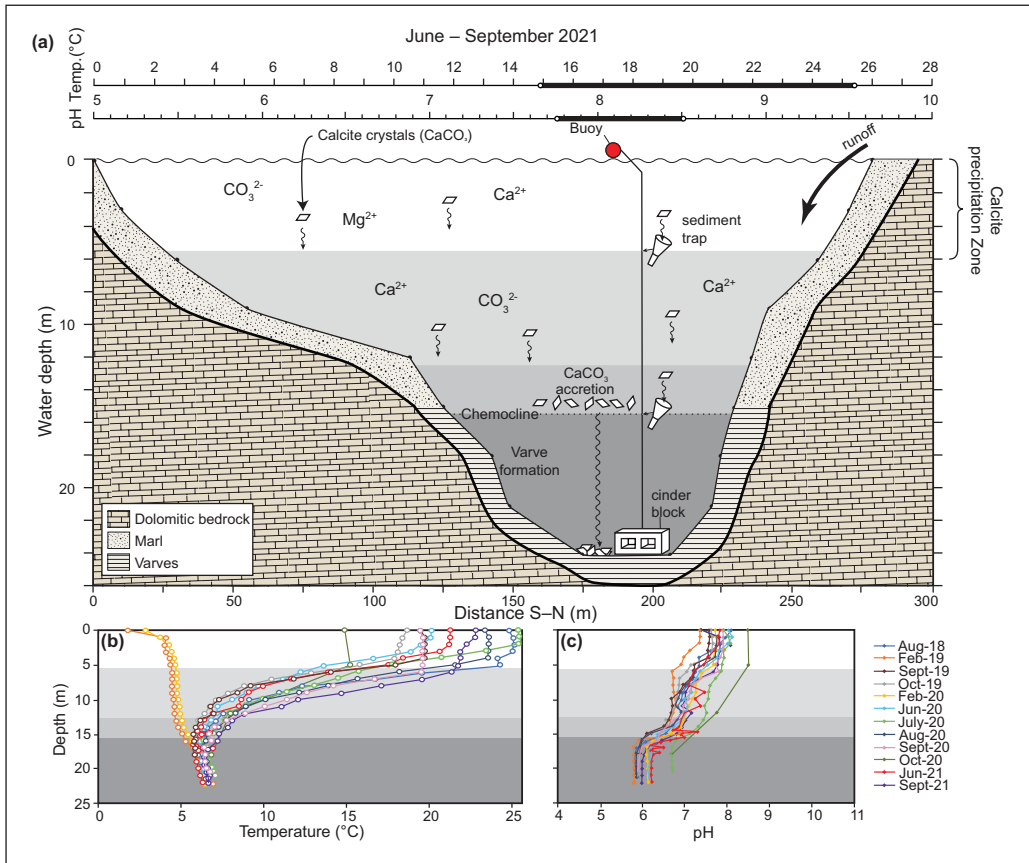


Figure 4. (a) Range of water temperature and pH required for calcite to precipitate in Crawford Lake, based on analysis of sediment traps and Langelier Saturation Index calculations. (b, c) These conditions were only met during summer and early fall in the upper 6 m of the water column. Crystals grow when they encounter Ca²⁺ and CO₃²⁻ saturated water along the chemocline where the density contrast slows their descent until they become large enough to overcome Stokes' Law and sink through the dense and slightly acidic monimolimnion to form the light-coloured summer varve couplet. Modified from Llew-Williams (2022). Reproduced in color in online version.

temperature exceeds 15°C and pH exceeds 7.7 (Figure 4), mainly when photosynthesis draws down free CO₂ and HCO₃⁻ levels, allowing calcium carbonate to precipitate. Crystals grow when their descent is slowed by the density increase at the chemocline (Llew-Williams, 2022), where the concentration of Ca²⁺ and CO₃²⁻ increases rapidly (Supplemental Figure S5). Crystals that survive the descent through the slightly acidic monimolimnion form a light-colored summer layer, allowing precise and accurate chronological resolution (Table S1, Supplemental Figure S9).

As the aquifers that transect the basin are recharged ~1 km up-dip (Figure 2 and Supplemental Figure S3), the groundwater is highly oxygenated (Llew-Williams, 2022). Dissolved oxygen (DO) values remained above the hypoxic limit (2 mg/l) throughout the water column between August 2018 and September 2021 (Figure 3e), and the monimolimnion of this unusual meromictic lake hosts metabolically active rotifers and cladocerans (Heyde, 2021; Mazumder, 1983; Supplemental Figure S4). The lack of bioturbation is attributed to the absence of benthos larger than microscopic nektonic ostracods in the slightly saline bottom water. These stygiogaunal (groundwater-dwelling) ostracods presumably reached the monimolimnion through aquifers in the karstic limestone (Heyde, 2021).

Table 1. Details of cores analysed to assess the varved sediments from the deep basin of Crawford Lake as a potential GSSP location for the Anthropocene.

Date of collection	Core name/type (F=freeze core face, G=gravity/UWITEC core)	Water depth (m)	Core length (cm)	Field crews	Analysis performed
2011/01/25	CL-2011 (F)	22.5	82	U. Toronto, Brock U., Conservation Halton	Radiocarbon/ bomb pulse; Palynology (pollen, NPP, microcharcoal and SCP), micro-XRF
2019/02/20	CRA19-2FT-IFR-A (F)	~22	88	Carleton U., Brock U., Conservation Halton	Radiocarbon (AMS- varve couplets)
2019/02/20	CRA19-2FT-B1 (F)	~23	83	Carleton U., Brock U., Conservation Halton	Siliceous microfossil (diatoms & chrysophyte scales)
2019/02/20	CRA19-2FT-B2 (F)	~22	107	Carleton U., Brock U., Conservation Halton	Varve imaging & SCP (+additional chrysophyte, radionuclide & stable isotope)
2019/02/20	CRA19-2FT-D1 (F)	~22	89	Carleton U., Brock U., Conservation Halton	Radionuclide & stable isotope (+additional diatom analysis)
2019/02/20	CL-19 (G)	22.1	116.8	Brock U., McMaster U.	Palynology (pollen, NPP, microcharcoal and SCP), micro-XRF, ²¹⁰ Pb, ¹³⁷ Cs, fossil pigments, C/N
2022/02/20	CRA22-IFR-1	17.4	68	Carleton U., Conservation Halton, Brock U.	Archived at ROM; being analyzed for ¹⁴ C (pollen concentrate) and SCPs in standard and palynological preparations, pollen and non-pollen palynomorphs
2022/02/20	CRA22-IFR-3	18.2	82	Carleton U., Brock U., CM	Archived in the National Biodiversity Cryobank of Canada, CMN; analyzed for plutonium, SCPs, gamma activity, and radiocarbon

Field collection of core, sampling, and core imagery

Most analyses presented in this article, including all key Anthropocene markers expected from all potential GSSP candidates, were performed on cores collected from the ice surface in February 2019 (Supplemental Figure S6). Details of the cores analyzed to assess the varved succession for defining the proposed Anthropocene series/epoch, as well as two subsequently collected and archived freeze cores, are summarized in Table 1 and additional information can

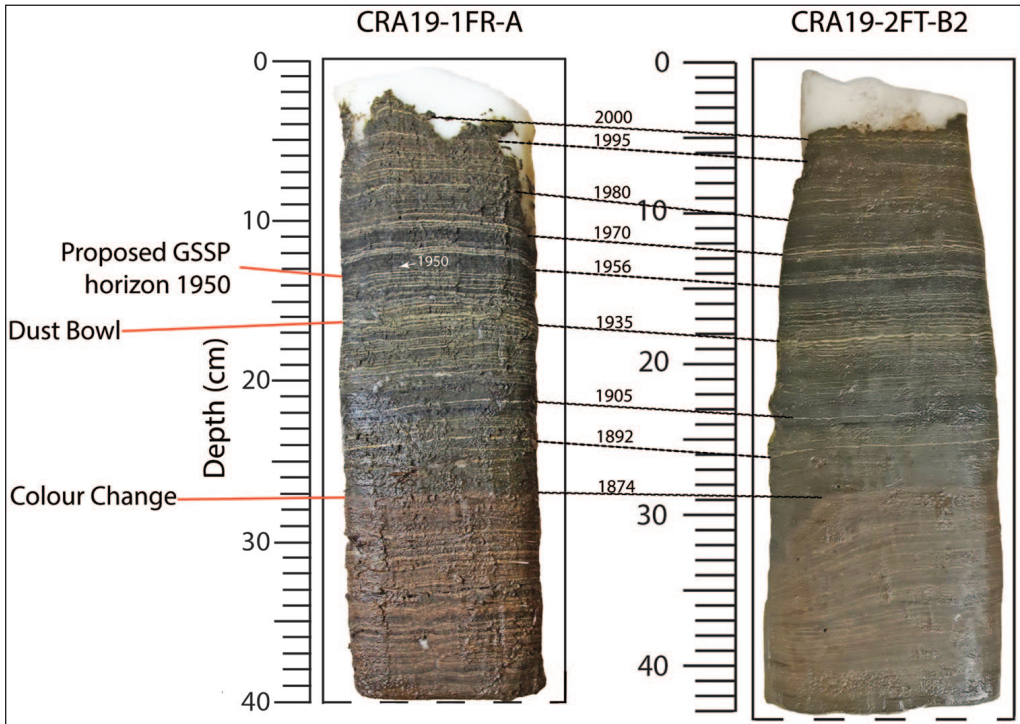


Figure 5. Freeze cores CRA19-2FT-1FR-A and CRA19-2FT-B2 collected from the deep basin of Crawford Lake in February 2019; see Supplemental Figure S6 for logs and images of cores CRA19-2FT-B1 and CRA19-2FT-D1. Dashed lines illustrate the ease with which varve-dated couplets can be correlated across freeze cores and the thin calcite lamina deposited in the summer of 1950 CE is indicated by the white arrow. Note that the loose sediments at the top of the cores were not recovered due to the short residence time of freeze corers in the substrate during the 2019 expedition, so varve ages were not determined by counting from the top but always with reference to the thickest white lamina assigned to 1935 CE, the warmest and driest year of the Dust Bowl interval; see Supplemental Table S1, Figure 7, and Supplemental Information for details of varve counting using high-resolution varve imaging (Supplemental Figure S9). Photo credit: K. Lafond. Reproduced in color in online version.

be found in the Supplemental Information. Additional cores may be collected from the lake with permission from Conservation Halton and must include consultation with Indigenous stakeholders.

Freeze cores identified as CRA19-“#-#” (Table 1, Figures 5, 6 and Supplemental Figures S6, S7) were collected on February 19 and 20, 2019 and kept frozen during transport to Carleton University. Cores were photographed and described both visually and using X-ray imagery. Cores CRA19-2FT-B2 and CRA22-1FR-3 received ultra-high resolution varve imagery and analysis (Figures 6 and 7).

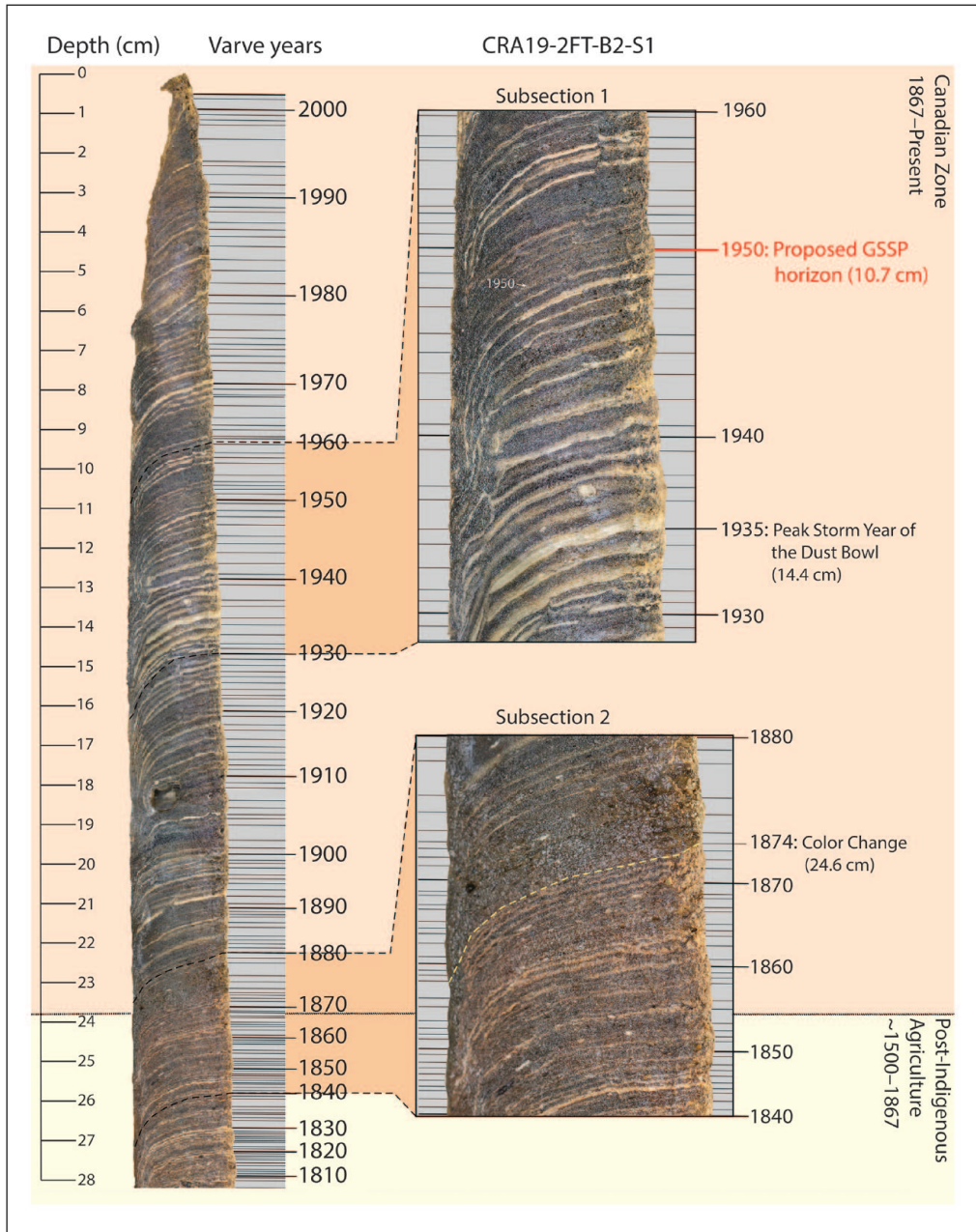


Figure 6. Composite image of a section (side-view) along core CRA19-2FT-B2 through the Canadian Zone (post-1867 CE); note curvature of horizontal varves as sediments froze onto the sampler as it sank slowly into the lakebed. The age model assumes that the thickest white lamina formed during the exceptionally warm, dry summer of 1935 CE (Lafond et al., 2022, Table S1). At this resolution, transition to and from the white “summer” layer includes substantial organic matter, whereas the center of the white layer consists almost entirely of calcite crystals. The first calcite lamina deposited during the proposed Anthropocene (1950 CE) is near the base of the lowermost of two dark intervals separated by a distinct triplet of varves dated to 1956, 1957, and 1958 CE (see Figure S9). Reproduced in color in online version.

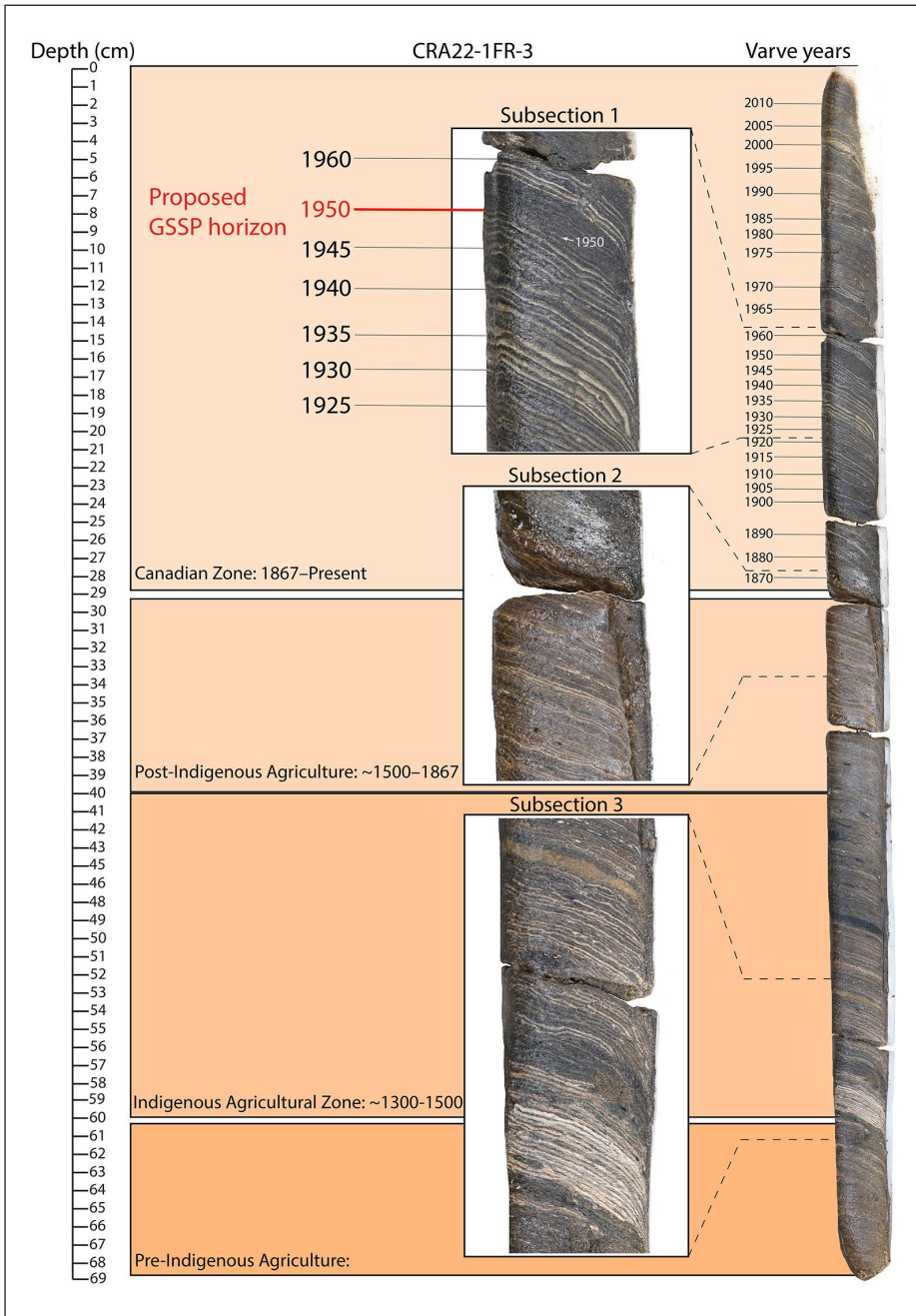


Figure 7. Composite image (side-view) of sections along the entire length of core CRA22-1FR-3, showing the position of the proposed GSSP. The uppermost enlargement allows the faint white lamina capping the 1950 CE varve year, at the base of the dark layer with almost imperceptible calcite laminae below the distinct triplet (varve ages 1956, 1957, and 1958 CE). The middle image shows the transition from reddish brown to very dark brown organic matter in the mid-19th century, when logging began. The lower enlargement illustrates the most prominent calcite laminae, deposited when an agricultural settlement was established during the Medieval Warm Interval (Llew-Williams et al., in revision). Reproduced in color in online version.



Figure 8. Section of core CL-2011, photographed during subsampling for radiocarbon analysis in 2018. This core was analyzed using micro-XRF and for additional palynological information including SCPs in “pollen slides,” with age model based on varve imagery (see Supplemental Information). Photo credit: F. McCarthy. Reproduced in color in online version.

All cores were subsampled for analysis of Anthropocene markers and siliceous microfossils along varve boundaries in freeze cores, following the varve chronology (Table S1, Supplemental Figure S9), but multiple varve years had to be amalgamated for many analyses depending on sample size requirements (see Table 1 and Supplemental Information, spreadsheet).

Samples extruded at 1 cm intervals in the field from core CL-19 collected using a UWITEC sampler were subsampled for plant macrofossils and palynological analysis at Brock University. Remaining sediment was analyzed using μ XRF at the ITRAX facility at McMaster University, then transported to the Paleoecological Environmental Assessment and Research Laboratory (PEARL, Queen’s University) for ^{210}Pb and ^{137}Cs activities by gamma spectrometry to develop an age model. Remaining sediment from core CL-19 was sent to the Institute of Environmental Change and Society, University of Regina for fossil pigment and stable isotope analysis.

Freeze core CL-2011 collected by a team from the University of Toronto in January 2011 (Figure 8) was kept in a chest freezer in the McCarthy Laboratory at Brock University. It was

subsampled in November 2018 by F. McCarthy for radiocarbon/ bomb pulse analysis at ETH, Zurich. It had previously been subsampled and analyzed for pollen and dinoflagellate cysts (Krueger, 2012; Krueger and McCarthy, 2016), and these and additional subsamples were analyzed for algal and consumer palynomorphs as part of this study (Heyde, 2021). The core thawed in 2021 but because it was mounted on plywood and stored horizontally the varve stratigraphy was intact. The thawed section around the proposed Anthropocene boundary was sent to the ITRAX facility at McMaster University for μ XRF geochemical analysis, and additional samples were processed for palynological analysis to compare directly with ITRAX measurements. These macerations were analyzed for pollen and black carbon (Moraal et al., in prep.) to provide additional chronological control for gravity core CL-19 that had been analyzed for these same proxies at Brock University (McCarthy Laboratory).

Freeze cores were collected from the ice surface on February 20, 2022, led by members of the Patterson Laboratory. A Wendat and Anishinaabe ceremony was performed by an Anishinaabe member of the team before, during, and after core collection under the guidance of Wyandot artist and elder Catherine Tammaro (Wong et al., 2020). The proposed GSSP (in core CRA22-1FR-3) is archived in the National Biodiversity Cryobank of Canada at the Canadian Museum of Nature (CMN), Ottawa; and the parastratotype (core CRA22-1FR-1) is archived at the Royal Ontario Museum (ROM), Toronto. Highly-resolved subsamples from trimmings of archived core CRA22-1FR-3 were submitted for additional plutonium, radiocarbon and gamma analysis, and radiocarbon analysis is to be performed on the terrestrially derived pollen fraction of core CRA22-1FR-1; palynological preparations from this core are being analyzed for black carbon at Brock University and University College London.

Cross-sections along the length of freeze cores CRA19-2FT-B2 and CRA22-1FR-3 were imaged at ultra-high resolution at Carleton University (Figures 6 and 7 and Supplemental Figure S9). Images were captured every 1 cm using a Canon EOS 6D Mark II equipped with a Canon EF 100 mm f/2.8L Macro IS USM lens and Canon Macro Ring Lite MR-14EXII mounted on a Cameron 120 cm CF camera rail slider. Images were cropped using Adobe Photoshop 2020 to their center third to minimize barrel distortion due to lens curvature and a single-profile image of each core was created by overlapping and matching characteristic sedimentary features, using the blending feature set to panoramic (Lafond et al., 2022; see Supplemental Information).

Chronological controls

As core tops are not always fully recovered (see Supplemental Figure S7), varve years were counted relative to clear marker laminae. Climate exerts a strong control on varve thickness (Supplemental Figure S10), so the thickest white lamina was attributed to the warmest, driest year of the “Dust Bowl” interval (1935 CE; see Supplemental Information for additional details about varve chronology and sampling) and all subsequent sampling used this baseline. Samples taken for radiocarbon analysis (Table 2) and siliceous microfossils in June 2019 (Gushulak et al., 2022) followed the chronology of Krueger (2012) that had assigned ages of 1953–1955 CE to three prominent white laminae near the center of a 2 cm-thick dark band in which the proposed base of the Anthropocene lies. Lafond et al. (2022) assigned ages of 1956–1958 CE to these laminae by counting laminae above the distinctive 1935 CE varve (Figures 6 and 7 and Supplemental Figure S9).

^{210}Pb analysis was employed to provide an age model for gravity core CL-19 at PEARL, Queen’s University. Twenty-eight sediment samples from the upper 39 cm of core CL-19 that had been extruded at 1-cm intervals in the field were analyzed using a germanium well detector to determine the activities of ^{210}Pb , ^{137}Cs , and ^{214}Bi (a proxy for ^{226}Ra) at PEARL (Queen’s University). The resulting gamma spectra were analyzed using the MATLAB program ScienTissME (<http://www.scientissime.net/software/>) using calibration standards (IAEA 285 and 312) and associated corrections for differences in tube height calibrated to these standards. The time-depth chronology was determined from unsupported ^{210}Pb activities using the constant rate of supply (CRS) model (Appleby and Oldfield, 1978) and

Table 2. Summary of radiocarbon analysis of bulk sediment and macrofossils (**bold**), with samples in stratigraphic/chronologic order (a) from core CRA19-2FT-1FR-A at the André E. Lalonde AMS Laboratory, U. of Ottawa and (b) from core CL-2011 at ETH, Zurich. The “bomb pulse” that compensated for the ~1100-year-old carbon attributed to Silurian dolomite is identified using gray shading; note, however, that $F^{14}C$ measurements of bulk sediments at ETH may retain some old carbon, attenuating the bomb pulse, so the macrofossil specimen from the 1981 to 1984 sample is probably a more accurate record of atmospheric radiocarbon than the sediment.

Lab ID	Submitter ID	Varve Count Age*	$F^{14}C$
UOC-12317	CRA19_IFRA_12	1975–78	1.4331 ± 0.0042
UOC-12312	CRA19_IFRA_1	1965–67	1.0825 ± 0.0031
UOC-12316	CRA19_IFRA_10	1958–61	1.0493 ± 0.003
UOC-12314	CRA19_IFRA_4	1952–53	0.8883 ± 0.0025
UOC-12315	CRA19_IFRA_6	1948–51	0.8658 ± 0.0025
UOC-12313	CRA19_IFRA_2	1933–37	0.8643 ± 0.0026
(a)			
ETH-96000	CL1990, 5 cm	1991–94	1.0349 ± 0.0027
ETH-95999	CL1980, 6.2 cm	1981–84	1.0756 ± 0.0028
ETH-101672	CL1980, MACRO	1981–84	1.1785 ± 0.0073
ETH-95998	CL1970, 9 cm	1971–74	1.1360 ± 0.0041
ETH-95997	CL1960, 11.5 cm	1961–64	1.0250 ± 0.0038
ETH-95996	CL1950, 12.5 cm	1951–54	0.8674 ± 0.0025
ETH-95995	CL1940, 15 cm	1941–44	0.8493 ± 0.0022
ETH-95994	CL1930, 16.5 cm	1931–34	0.8501 ± 0.0036
ETH-95993	CL1920, 19.8 cm	1921–24	0.8430 ± 0.0023
ETH-101671	CL1920, MACRO	1921–24	0.8318 ± 0.0063

*Varve count age follows the age model of Lafond et al. (2022), 3 years younger than submitted varve ages. See Supplemental Information for details.

the well-defined *Ambrosia* rise at 23 cm as an anchor point (1830 ± 20 CE). Pollen analysis conducted at Brock University identified the rise in *Ambrosia* (ragweed pollen) at 23 cm, dated 1830–1840 CE at Crawford Lake (Ekdahl et al., 2004), which reflects colonial land disturbance. Historic records of logging and Dutch elm disease, first identified in Ontario in 1946 (<https://www.ontario.ca/page/dutch-elm-disease>) helped further date changes in pollen spectra by comparison with published records from varved samples (e.g. McAndrews and Turton, 2010). The decline in elm pollen could be a useful marker for the base of the proposed Anthropocene throughout eastern North America. In Crawford Lake, this event is accompanied by an increase in pine pollen and decrease in non-arboreal pollen following a cessation of logging in the early 1900s (Supplemental Figure S11).

Anthropocene proxies

Accelerator mass spectrometer (AMS) radiocarbon analysis of bulk varved sediment from cores CL-2011 and CRA19-1FR-A was performed at ETH, Zurich (Synal et al., 2007) and André E. Lalonde (AEL) AMS Laboratory, University of Ottawa (Crann et al., 2017), respectively. Samples were treated with acids (80°C at AEL and 60°C at ETH) to remove carbonates and bases to remove humic acid contamination (Crann et al., 2017; Hajdas et al., 2021). Two macrofossils were found in bulk sediment of CL-2011 and analyzed using the gas ion source at ETH Zurich (Ruff et al., 2010). Radiocarbon ages

were calculated as $-8033\ln(F^{14}\text{C})$ following Stuiver and Polach (1977), with the fraction modern carbon ($F^{14}\text{C}$) calculated following Reimer et al. (2020) and reported in ^{14}C year BP (BP= 1950 CE). $F^{14}\text{C}$ values were compared to the atmospheric record of the Northern Hemisphere (Hua et al., 2022).

Spheroidal carbonaceous particles (SCPs) were extracted from samples following Rose (1994) from core CRA19-2FT-B2 at University College London. Dried sediment was subjected to sequential chemical attack by mineral acids leaving a suspension of mainly carbonaceous material and a few persistent minerals. A known fraction of the final suspension was evaporated onto a coverslip and mounted onto a microscope slide. Analytical blanks and SCP reference material (Rose, 2008) were included in the sample batch. The SCPs on the coverslip were counted and subdivided into size classes using a light microscope at $400\times$ magnification and calculated as the number of particles per gram dry mass of sediment (g/DM). Criteria for SCP identification followed Rose (2008). Black carbon, including SCPs, was also identified in “pollen slides” from freeze core CL-2011 and gravity core CL-19 at Brock University (Moraal et al., in prep.). Methods and criteria used to differentiate SCPs from microscopic charcoal and other black carbon in palynological preparations can be found in the Supplemental Information.

Homogenized subsamples were analyzed on an elemental analyzer (ANCA GSL, Sercon, UK), combusted over chromium(III) oxide at 1000°C and reduced over activated copper at 600°C . Water was removed using a magnesium perchlorate scrubber and N_2 and CO_2 were separated using gas chromatography. Isotopic ratios and quantifications were determined using a mass spectrometer (20-20MS, Sercon, UK). Certified standards calibrated against IAEA-CH-6 and IAEA-N-1 (Elemental Microanalysis, Oakhampton, UK) were measured every nine samples and a blank correction was applied to all nitrogen analyses. Total nitrogen (TN) and organic carbon (TOC) are expressed in mass as percentage values, C:N ratios were calculated on a mass basis, and stable isotopic composition relative to the standards were expressed in permille values using delta notation: $\delta X = [(R_{\text{sample}}/R_{\text{standard}}) - 1] \times 100$, where δX is $\delta^{13}\text{C}$ versus V-PDB or $\delta^{15}\text{N}$ versus air, R is the $^{13}\text{C}/^{12}\text{C}$ or $^{15}\text{N}/^{14}\text{N}$ ratio. Precision and accuracy was 0.1 permille for both $\delta^{15}\text{N}$ and $\delta^{13}\text{C}$. Analysis of samples from core CL-19 was performed at the University of California, Davis, using the same standard protocols (see Supplemental Information).

Plutonium (Pu) was also measured on varved samples from cores CRA19-2FT-D1 (with additional sediment from the portion of core CRA19-2FT-B2 previously imaged at high resolution) at the GAU-Radioanalytical Laboratories, University of Southampton. The inorganic fraction after ignition at 450°C was spiked with ^{242}Pu chemical recovery tracer, mixed with lithium metaborate flux and fused at 1100°C to achieve a homogenous melt. The obtained liquid glass was quenched in deionized water and then dissolved in 8M HNO_3 at 90°C . After cooling to room temperature, the resulting boric acid precipitate was filtered off using a GF/A filter paper. Pu was pre-concentrated from the sample solution by means of co-precipitation with $\text{Fe}(\text{OH})_3$ at pH 5–6, separated by centrifuging and re-dissolved in 9M HCl . The 9M HCl solutions were transferred to anion exchange columns. The Pu fraction was eluted to pre-cleaned beakers using 40 ml of $0.1\text{M NH}_4\text{I}/9\text{M HCl}$ solution and evaporated to dryness. Thin alpha spectrometric sources prepared by electrodeposition were counted using Octete alpha spectrometers equipped with PIPS detectors. Resulting spectra were analyzed using Maestro spectral analysis software. $^{240}\text{Pu}/^{239}\text{Pu}$ ratios were determined using a Thermo Scientific Neptune Plus MC-ICP-MS after radiochemical re-purification of the Pu alpha spectrometry disks, following Łokas et al. (2022).

Micro-XRF geochemical analysis was performed on gravity core CL-19 and freeze core CL-2011 at McMaster University using an ITRAX core scanner outfitted with a Cr tube. A representative portion of each 1-cm subsample from core CL-19 was loaded into a sampling tray (Gregory et al., 2017) and run with $500\ \mu\text{m}$ sample interval, 15 seconds exposure time and $30\text{ kV}/30\text{ mA}$ power settings. Core CL-2011 was run intact with $200\ \mu\text{m}$ sample interval, 25 seconds exposure time, and $30\text{ kV}/25\text{ mA}$ power settings. Spectra were batch analyzed using QSpec™ software, and element profiles were normalized using the ratio of coherent to incoherent scatter (Gregory et al., 2019).

Samples aggregating 2–3 varve years between the early 19th and 20th centuries from core CRA19-2FT-B1 were processed for siliceous microfossil analysis at Queen's University (Gushulak et al., 2022; Marshall, 2021) following the methodology of Battarbee et al. (2001). Diatom valves and chrysophyte scales were identified and enumerated using a Leica DMRB microscope with an oil immersible Fluotar objective using DIC (differential interference contrast) at 1000 \times magnification; identifications were to the lowest taxonomic resolution possible using numerous guides (see Supplemental Information). Annual couplets from 1930 to 1990 CE from core CRA-19-2FT-D1 were processed using the same protocol and analyzed at Carleton University and at the Canadian Museum of Nature (Marshall et al., 2023).

Samples from UWITEC gravity core CL-19 (Supplemental Figure S8) and freeze core CL-2011 (Figure 8) were processed for palynological analysis at Brock University using a modified technique that omits the use of strong oxidants and bases to avoid destroying susceptible non-pollen palynomorphs (McCarthy et al., 2021). Mineral sediment was dissolved using HCl and HF, and residues were sieved using a 15 μ m Nitex[®] mesh prior to mounting on glass microscope slides with glycerine jelly. Slides were analyzed at 400 \times magnification for pollen and non-pollen palynomorphs (NPP) primarily using the guides of McAndrews et al. (1973) and McCarthy et al. (2021).

Fossil pigments were analyzed on core CL-19 at the University of Regina. Fossil pigment concentrations were measured using an Agilent model 1100 HPLC equipped with a photodiode array spectrophotometer which was calibrated using authentic standards and Sudan II as an internal reference standard. Identification of chlorophylls, carotenoids, and derivative products was based on the taxonomic assignment of Leavitt and Hodgson (2001) using chlorophyll *a* derivative pheophytin *a* as a biomarker of total phototroph production. All pigment concentrations were expressed as nmoles pigment/g dry mass. The ratio of chlorophyll *a* to pheophytin *a* (chl *a*:pheo *a*) is a metric of changes in the preservational environment (Leavitt and Hodgson, 2001).

Numerical analysis

Numerical analyses employed to interpret the results in the following section are described in the Supplemental Information, together with additional details of methodologies summarized above.

Results

Lithology

All cores show a marked color change from reddish brown sediments to very dark brown organic matter at ~25 cm depth (Figures 5–8). Varves are composed of authigenic organic matter capped by calcite precipitated inorganically in the epilimnion/uppermost hypolimnion (see Figure 4). Pale-colored, thin (most <1 mm) calcite laminae punctuate the organic matter, more prominently in the upper 25 cm and again at ~45–65 cm, highlighted by X-ray imagery (Supplemental Figure S7 and Table S1). Within the generally richly calcitic upper 25 cm are several nearly centimeter-thick bands with barely perceptible white laminae separated by a triplet of prominent calcite laminae (e.g. 12–19 cm in core CRA19-2FT-B2; Figures 5 and 6). Silicates are a small fraction of the sediments but small quantities of clay to very fine sand-sized quartz were noted during palynological processing, primarily in the intervals with prominent calcite laminae. Macrophyte remains are sporadically present, most abundantly in droppings of Canada geese

that occasionally distort the laminae, particularly where local agriculture is evident in the palynological record (McAndrews and Turton, 2007). Varve couplets are undisturbed by bioturbation, even though the monimolimnion is well-oxygenated (Heyde, 2021). The distinctive varves are easily correlated across the deep basin of Crawford Lake (Figure 5 and Supplemental Figure S7) reflecting climate and eutrophication (Llew-Williams, 2022 and Llew-Williams et al., in revision; see Supplemental Information).

It was not possible to photograph core CL-19 before subsampling in the field, but physical properties were measured on 1-cm subsamples prior to gamma ray analysis at Queen's University (Supplemental Figure S8 and Table S2). Dry bulk density is very low (mean DBD = 0.96, $n = 28$, range 0.06–0.17 g/cm³) and sediments are highly porous (0.94–0.98 on a scale of 0–1). The uppermost sample is anomalous, with the highest DBD and lowest porosity likely an artifact of capping of the core tube to prevent loss of sediment through degassing, a common issue with recovering all but freeze cores from the deep basin of Crawford Lake (Heyde, 2021).

Chronology

Ultra-high-resolution imagery of cores CRA19-2FT-B2 and CRA22-1FR-3 (Figures 6 and 7) illustrates the distinctive varve pattern that allows correlation across the deep basin of Crawford Lake and permitted subsampling of freeze cores by varve years. It also confirms the climatic control and seasonality of calcite deposition (Supplemental Figure S10), with gradation from almost pure calcite to increasingly dark sediments (visible in thick varves like that deposited in 1935; see Supplemental Figure S9) characterizing fall turnover, when plankton remains sink rapidly to the lakebed through a nearly isothermal water column (Llew-Williams, 2022; Llew-Williams et al., in revision). Direct observation of freeze cores collected since the early 1970s and high-resolution AMS ¹⁴C chronology confirms that these represent annual couplets through the Canadian zone (Ekdahl et al., 2004), allowing varves from the past 150 years to ensure accurate and precise correlation between freeze cores.

Age control for conventional gravity core CL-19 relies primarily on the activity of short-lived radionuclides and regional pollen stratigraphy since laminations are not easily discriminated with annual precision. The activity of ²¹⁰Pb shows a strong first-order exponential decay through the core ($R^2 = 0.93$), and a discrete peak in ¹³⁷Cs is present around 10.5 cm (Figure 9 and Supplemental Table S2). The sharp rise in *Ambrosia* (ragweed pollen) at ~23 cm (Figure 10), dated 1830–1840 CE by varve counting, supported by several AMS dates (Ekdahl et al., 2004; McAndrews, 1994) is an additional constraint. This is consistent with other proxies that were analyzed in palynological samples from this core and in freeze core CL-2011, where the 1950 CE couplet is easily discerned near the base of a dark unit in the core marked by thin calcite laminae attributed to acid precipitation accompanying the Great Acceleration (see Figure 14). The ²¹⁰Pb age model for the gravity core suggests that the mean rate of sedimentation through the Canadian Zone (since 1867 CE) was 1.48 mm/year or 6.76 years/cm. This is lower than the mean accumulation rate (MAR) of 1.82 mm/year (or 5.49 years/cm) estimated between 1870 and 2000 CE in freeze core CRA19-2FT-B2 (see Supplemental Table S1 and Figure S12) or the estimate of nearly 2 mm/year in a freeze core studied by Ekdahl et al. (2004). While these sedimentation rates are very low compared to most lakes, they are higher than in lower parts of the succession in the deep basin of Crawford Lake; Ekdahl et al. (2004) estimated accumulation rates <0.4 mm/year between 1486 and 1867 CE, and ~0.5 mm/year was estimated for the post-Indigenous Agriculture zone based on the pollen record of core CL-19 (Figure 11a).

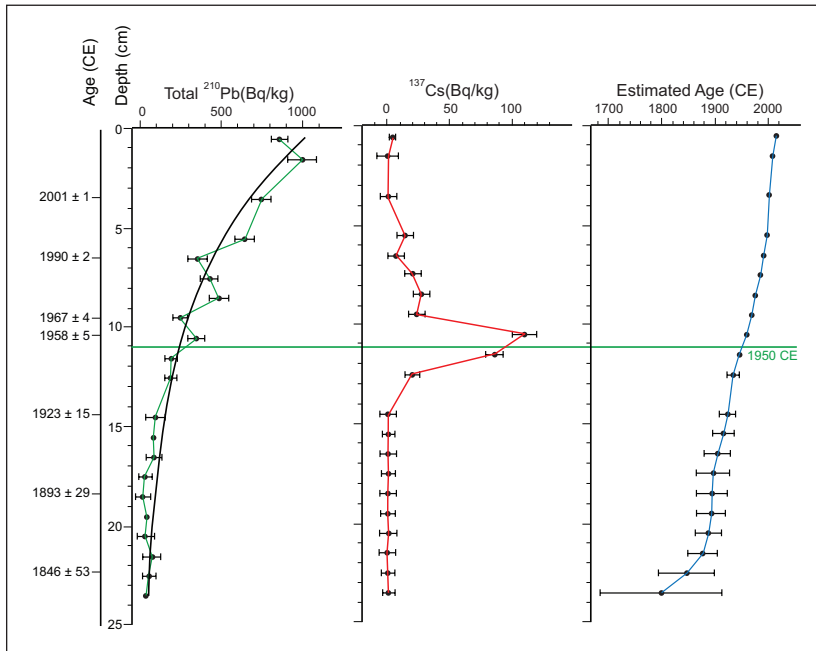


Figure 9. Activities of total ^{210}Pb and ^{137}Cs and associated counting error measured approximately every 1 cm from the CL-19 gravity core measured by gamma spectroscopy (Supplemental Table S2). The modelled ages are based on a constant rate of supply model on the estimated unsupported ^{210}Pb activity constrained to a tie point at 23 cm (the *Ambrosia* rise, that was set at 1830 CE \pm 20 years). Background (supported) ^{210}Pb activities were estimated from the mean of the bottommost 7 samples for total ^{210}Pb activities in the CL-19 core (14.8 Bq/Kg \pm 3.2) which was similar to the tail of the total ^{210}Pb activities in this core (10.8 Bq/Kg \pm 10.7, n=7). The correspondence of the ^{137}Cs peak in the early 1960s CE supports the age estimates of the CRS model (Supplemental Table S3). Reproduced in color in online version.

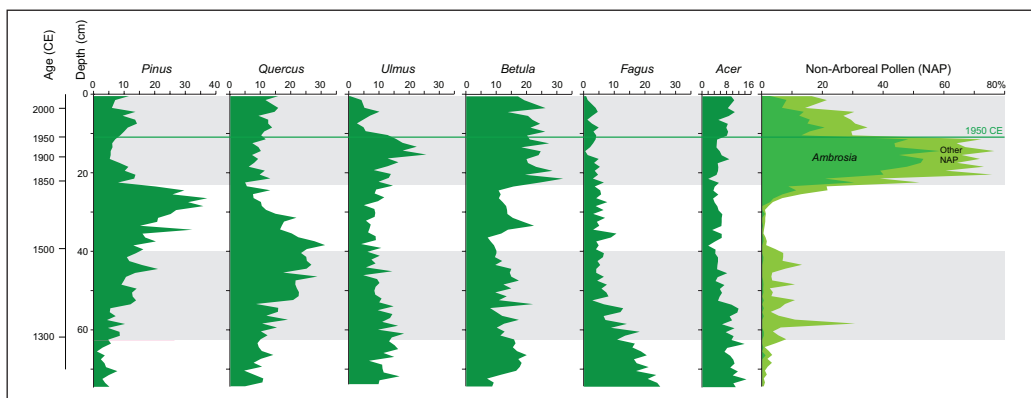


Figure 10. The rapid decline in *Ulmus*, marking the effects of Dutch elm disease, regionally identifies the base of the proposed Anthropocene series/ epoch (compare with varve-age dated pollen spectra over the last millennium, Supplemental Figure S11). The pollen zonation reveals the much lower rates of sediment accumulation between the intervals of human impact on the Crawford Lake catchment indicated by stippling. An anomalous peak in pine pollen (*Pinus*) followed by a peak in early successional taxa such as birch (*Betula*) suggests disturbance during the Little Ice Age, probably by fire. This anomaly was also identified in a freeze core record by McAndrews and Turton (2010) in sediments dating to the early 18th century. Reproduced in color in online version.

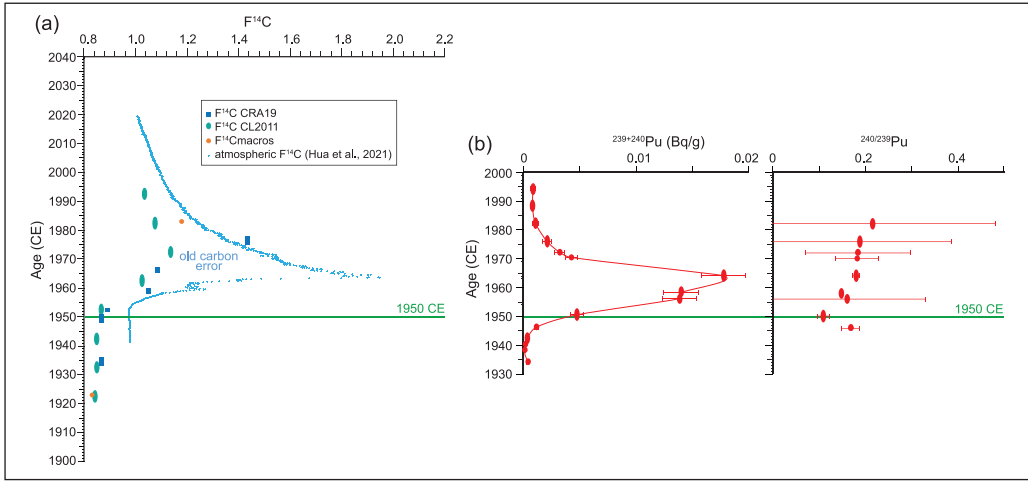


Figure 11. Anthropogenic radiogenic signatures in varved sediments from Crawford Lake, calendar year using varve chronology (Table S1, Figure S9) with horizontal line identifying 1950 CE. (a) Values of $F^{14}C$ in bulk sediment from core CRA19-2FT-1FR-A and macrofossils from core CL-2011 (Table 2) compare well with atmospheric ^{14}C concentration (Hua et al., 2022). In addition to old carbon found in DOC and POC throughout the water column (Table S5), bulk sediment samples from core CL-2011 probably retain some dolomitic old carbon because of incomplete digestion. Nonetheless, values of $F^{14}C > 1$ were measured through the post-bomb era, identifying the “bomb pulse” of artificially created radiocarbon. (b) Activity of $^{239+240}Pu$ (with counting error) in sediments subsampled by varve age from core CRA19-2FT-D1, supplemented by Pu material from core CRA19-2FT-B2 mirrors the global signature of atmospheric deposition of plutonium from above-ground nuclear testing (United Nations Scientific Committee on the Effects of Atomic Radiation (UNSCEAR), 2000). Reproduced in color in online version.

Radioisotopes

Radiocarbon. Radiocarbon results are affected by excess stable carbon isotopes attributed to abundant carbon dissolved from Silurian bedrock in the Crawford Lake ecosystem (see Supplemental Information) but the “bomb pulse” (Radowsky et al., 2013) is obvious in samples where the fraction modern carbon ($F^{14}C$) revealed the presence of artificially produced radiocarbon, that is, values of $F^{14}C > 1$ (Table 2 and Supplemental Tables S4–S6). This includes samples with varve ages 1958–1961, 1965–1967, and 1975–1977 CE in sediment samples from core CRA19-2FT-1FR-A and sediments dated 1961–1964, 1971–1974, 1981–1984, and 1991–1994 CE from core CL-2011 (ages corrected to conform with final varve age model, Table S1, Figure S9). The higher $F^{14}C$ in the macrofossil from the 1981 to 1984 CE sample from core CL-2011 is probably a more accurate measure than that of the bulk sediment in which it was found. The values, with a peak in 1970 CE, compare reasonably well with the post-bomb atmospheric curve of Hua et al. (2022), taking the attenuation of $F^{14}C$ in bulk sediments measured at ETH into account (Figure 11a). Values of $F^{14}C < 1$ were measured for all other samples.

Plutonium. A sharp increase in $^{239+240}Pu$ activity was identified beginning between 1948–1951 and 1950–1953 CE (samples plotted as ellipses to portray the variable number of varve years combined for analysis, with analytical error indicated at the midpoint of the sample). Activity continued to increase sharply to the sample from 1956–1957, slowing to 1958–1961, and rising

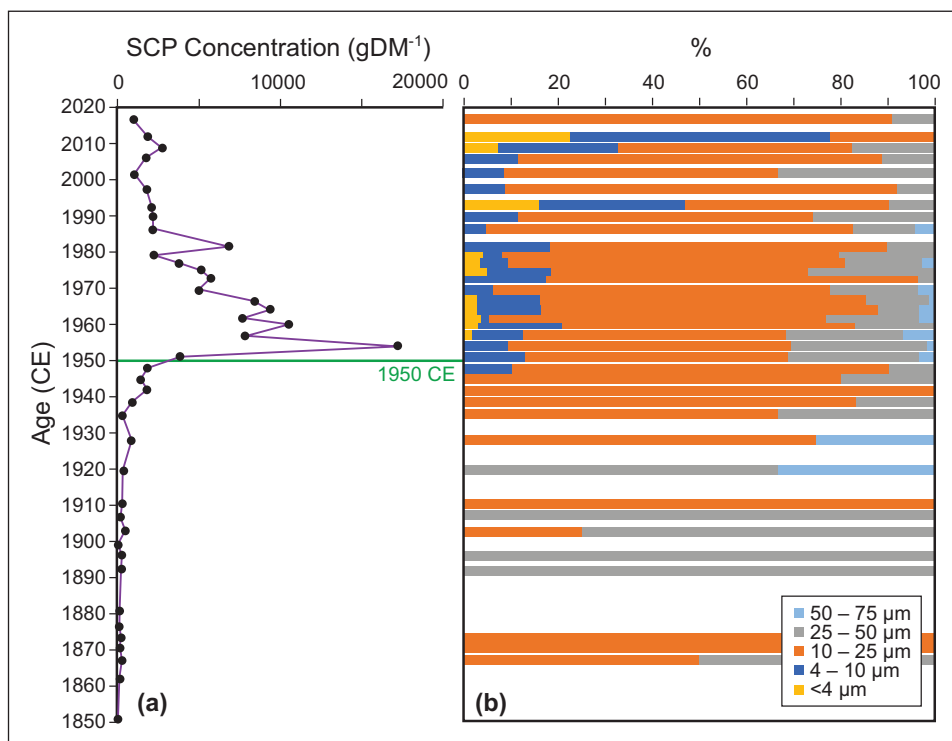


Figure 12. SCPs in core CRA19-2FT-B2. (a) Concentrations increase sharply between 1948 and 1954 CE. (b) Particles larger than 10 μm occur throughout, while smaller particles gradually increase in abundance after 1945 CE. The decline in SCPs larger than 25 μm coincides with closure of the lumber mill at Crawford Lake in 1900 CE. The proposed base of the Anthropocene is shown at 1950 as a solid horizontal line. Reproduced in color in online version.

quickly again to a peak in the sample from 1964–1967 CE. This was followed by a sharp drop, reaching the Nuclear Age plateau by 1982–1985 CE (Figure 11b and Supplemental Table S8). Plutonium isotope ratios ($^{240}\text{Pu}/^{239}\text{Pu}$) over the mid-1950s–1980s period ranged between 0.15 and 0.19, consistent with ratios previously reported for global weapons fallout in mid-high northern latitudes (Wu et al., 2011).

Novel materials

Fly-ash. Spheroidal carbonaceous particles (SCPs) are a particulate by-product of high temperature, industrial combustion of coal-series and oil fuels. They are morphologically distinct (Supplemental Figures S17 and S18) making them unambiguous indicators of deposition from these sources (Rose, 2015). SCPs spanning a range of sizes were present in core CRA19-2FT-B2 between 1868 and 2019 CE, peaking in concentration in the sample from 1953–1955 CE. A gradual rise from ~ 1800 g/DM in 1941–1943 to ~ 3800 g/DM in 1950–1952 was followed by a rapid rise to a peak of $\sim 17,000$ g/DM in 1954 CE. Concentrations sharply declined to ~ 8000 g/DM by 1967, stabilizing between ~ 1000 and 2000 g/DM after 1980 CE (Figure 12a and Supplemental Table S9). Smaller fractions (<4 – 10 μm) were present only in samples deposited after 1945 whereas particles larger than 25 μm were most abundant between 1893 and 1929 CE (Figure 12b and Supplemental Table S10). A similar trend was recorded by black carbon identified as SCPs in cores CL-2011 and CL-19 (Supplemental Figure S19

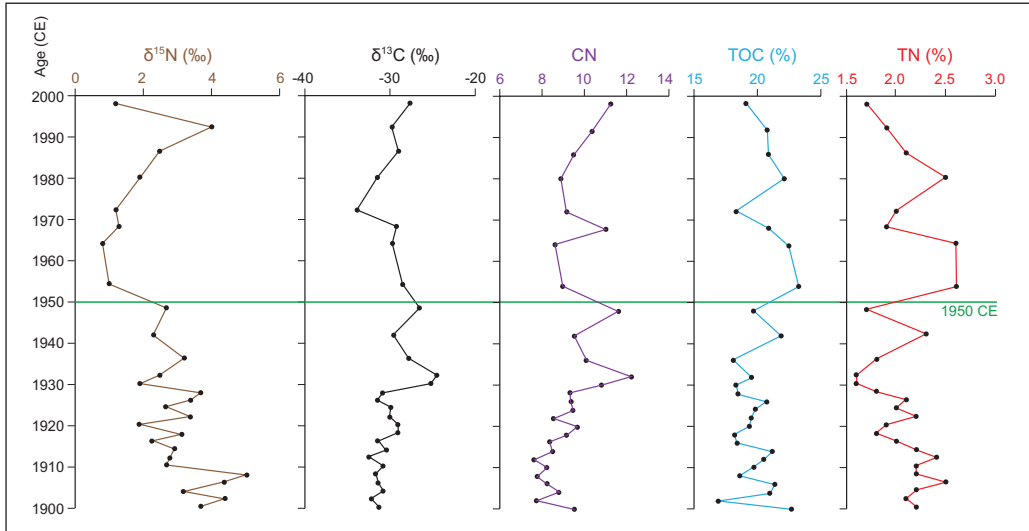


Figure 13. Organic proxies in sediments subsampled by varve age from core CRA19-2FT-D1, supplemented by material from core CRA19-2FT-B2. Sharply depleted values of $\delta^{15}\text{N}$ mark the proposed base of the Anthropocene epoch (1950 – horizontal line). High values of TN and TOC are in dark calcite-poor sediments that characterise the 1950s and 1960s (see Figures 5, 14), attributed to acidic precipitation. Reproduced in color in online version.

and Table S11) but because samples were sieved at $15\ \mu\text{m}$ during palynological preparation, it was not possible to discriminate the $<10\ \mu\text{m}$ fraction (see Supplemental Information).

Organic matter proxies

In 28 samples deposited between 1900 and 1999 CE, TOC values range from 16.9% to 23.3% (mean=20.1%), with the highest value in the sample from 1954–1955 CE (Figure 13 and Supplemental Table S12). These values were not unexpected in organic laminae capped by calcite. TN values were much lower, 1.6%–2.6% (mean=2.1%), with highest values in dark sediments with thin calcite laminae deposited in 1954–1955 and 1964–1965 CE (see Supplemental Figure S5). Parts of core CRA19-2FT-D1 with thick, prominent white laminae (e.g. the 1930s) had below average TOC and TN values. The highest C/N value, 12.2, was measured in the sample from 1932–1933, whereas samples from 1954 and 1964 were below the mean (9.4); the lowest C/N value, 7.6, was in the sample deposited in 1912–1913 CE.

Values of $\delta^{15}\text{N}$ declined to a minimum in the sample dated 1964–1965 CE before rising to a secondary maximum of 4 ‰ in the upper part of the core (~1992) (Figure 13). Values of $\delta^{13}\text{C}$ through the Great Acceleration (Head et al., 2022; Steffen et al., 2015) ranged from -34.0 in 1972–1973 to -24.6 ‰ in 1932–1933 (mean -29.9 ‰, $n=28$), with the most enriched values measured through the 1930s and 40s, following depleted values between 1900 and 1930 CE. These values are depleted compared to many temperate lakes, but they are characteristic of lakes with important sources of respired CO_2 , and they are comparable to values (-37.0 to -27.9 ‰) reported by Han and Dickman (1995) in a core from 21 m depth in Crawford Lake.

Similar results were obtained from gravity core CL-19, analyzed over the past 700 years (Supplemental Table S13 and Figure S17). Because subsamples average each centimeter along the core, the signature in the mid-20th century is muted; however, as in the freeze core record, depleted values of $\delta^{15}\text{N}$ are succeeded by less depleted values.

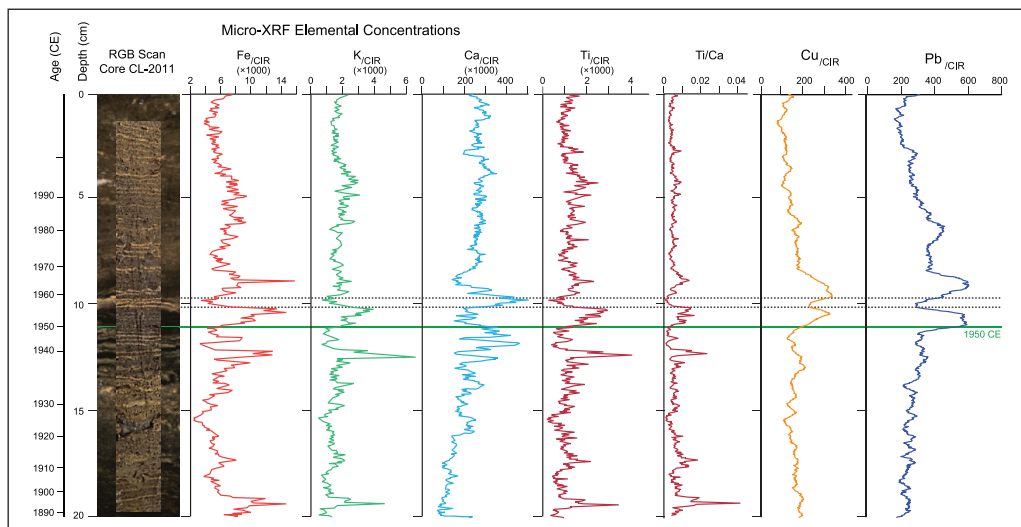


Figure 14. Laminae visible in the original core photo (Figure 6) superimposed on the ITRAX-generated RGB scan allow sediment geochemistry determined using μ XRF analysis of freeze core CL-2011 to be related directly to the varved sediments. Peaks in activity attributed to Cu and Pb peak around the proposed base of the Anthropocene where SPCs rich in these metals are abundant (see Figure 12). Peaks in activity attributed to Ca align with prominent light-coloured laminae (with prominent laminae deposited during the summers of 1956, 1957 and 1958 CE identified across the diagram by dashed lines) whereas peaks in terrigenous elements, such as Fe, K and Ti in dark layers record enhanced leaching of the catchment. Compare the μ XRF record in the upper 20 cm of gravity core CL-19 (Figure S21). Reproduced in color in online version.

Inorganic geochemical signals

μ XRF elemental analysis. Elemental analysis of thawed freeze core CL-2011 at 0.2 mm resolution revealed alternations between terrigenous elements (e.g. Fe, K, and Ti) and authigenic Ca (Figure 14). Both the ITRAX RGB image and the original photograph of the core correlate the sharpest peak in Ca with the triplet of prominent white laminae (see Supplemental Figure S9) at ~10 cm dated 1956, 1957, and 1958 CE. Elevated Ca values are associated with thick white laminae in the 1930s (the Dust Bowl), as are increases in terrigenous elements: iron, titanium, and potassium. Terrigenous elements are also more abundant in dark sediments with very thin white laminae during the mid-20th century (Figure 14). The Cu and Pb curves closely resemble each other, but while peaks in copper and lead characterize the mid-20th century, they do not correspond to the other peaks in iron, titanium and potassium. High activity attributed to copper and lead probably reflects industrial influx, specifically from the industrial city of Hamilton west of Crawford Lake. This is supported by chemical analysis of spheroidal carbonaceous particles (SCPs) by Lan and Breslin (1999). They found fly-ash to be responsible for up to 22% of the lead and 12% of the copper in sediments in western Lake Ontario, which increased in abundance through the 20th century, peaking in the 1970s (see Supplemental Figure S2).

Two distinct phases of terrigenous sediment influx are evident in the upper 26 cm of core CL-19 and between ~39 and 66 cm, corresponding to intervals of human impact (Supplemental Figure S20). The latter interval represents land disturbance during the Indigenous agricultural settlement phase (Ek Dahl et al., 2007), recorded by pollen of cultigens and spores of their pathogens (Figure 10 and Supplemental Figure S18). The peak in Fe, K, and Ti at ~22 cm in the colonial–Canadian interval in core CL-19 (~1850 CE) correlates with the base of the section analyzed in core CL-2011 (~20 cm) (Figure 14 and Supplemental Figure S20). Peaks in these elements relative to authigenic

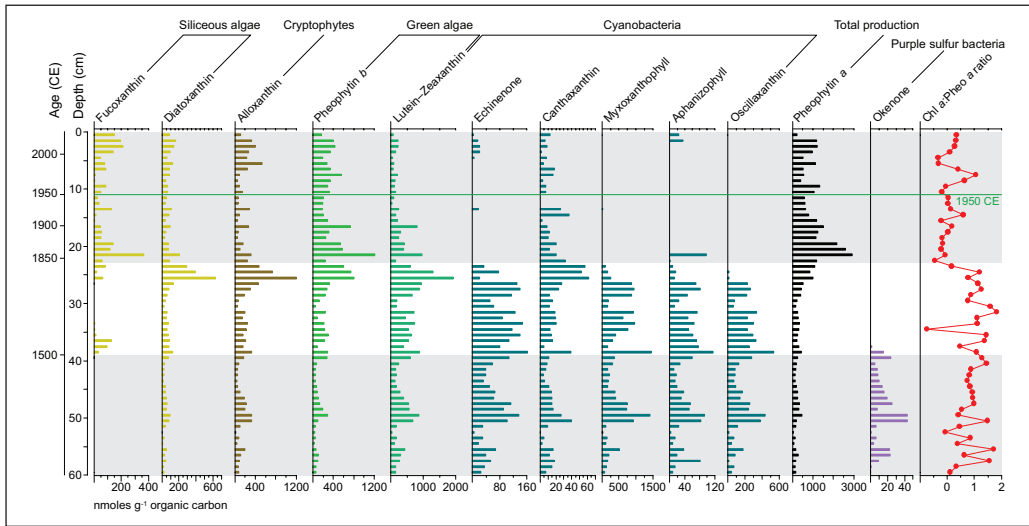


Figure 15. Summary fossil pigment concentrations in core CL-19 – note the absence of okenone above 38 cm, recording the unusual absence of anoxia in this meromictic lake since the early 16th century. The ratio of chlorophyll a (not plotted individually) to pheophytin a (Chl a : pheo a ratio) suggests poor preservation in the sample from 35 cm where an anomalous peak in resistant and readily transported pine pollen was identified (see Figure 10). Gray shading identifies intervals of human impact, Indigenous and colonial-Canadian. Reproduced in color in online version.

calcite are clearly depicted in the ratio of Ti/Ca in calcite-poor sediments between ~8 and 13 cm, that is, around 1950 CE. The similar concentration of iron, potassium, and titanium during the interval of Indigenous agricultural settlement and during the 20th century suggests that these terrigenous elements record increased runoff from the catchment (Rothwell and Croudace, 2015).

Biotic markers

Acid-resistant remains of invertebrate animals and protozoans were identified in the analysis of palynological preparations from cores CL-2011 and CL-19. Assemblage changes in the mid-20th century include an increase in the cladoceran genus *Daphnia* versus *Bosmina*, increased abundance of loricae of the rotifer *Keratella quadrata*, and a decline in *Keratella cochlearis* and *Kellicottia longispina* (Supplemental Figure S20). Palynological remains of eukaryotic algae in the same slides show major assemblage changes in the mid-20th century, with a decline in dinoflagellates and green algae (chlorophytes), particularly in contrast to the 19th century. Loricae of the chrysophyte *Dinobryon divergens* (Supplemental Figure S18), not previously reported in the literature, are extraordinarily abundant in palynological preparations spanning the mid-20th century to the modern day (Supplemental Tables S12 and S13). Cellulosic thecae of several dinoflagellate species are another unusual constituent in palynological preparations of the Crawford Lake *Konservat-Lagerstätte*, primarily from the mid-19th through early 20th century (Krueger and McCarthy, 2016).

Analysis of fossil pigments reveals two distinct associations corresponding to abundant cyanobacteria before ~1850 CE, and more common eukaryotic algae (siliceous algae, dinoflagellates and chlorophytes) afterwards (Figure 15). The transition marked by elevated concentrations of most pigments coincides with the onset of regional logging (Boyko, 1973). The absence of okenone from obligately-anaerobic purple sulfur bacteria after abandonment of the Indigenous agricultural settlement records well-oxygenated deep waters since ~1500 CE.

Constrained cluster analysis of the siliceous microfossil dataset spanning the early 19th through early 21st centuries identified a sharp increase in the scaled chrysophyte genus *Synura* relative to the otherwise dominant genus *Mallomonas* in the mid-20th century (Figure 16), with abundant *Mallomonas acaroides* var. *acaroides* from ~1950 CE to the top of the core section (Gushulak et al., 2022; Marshall et al., 2023). Increases in non-planktonic diatom taxa drive a major change in diatom assemblages at ~1942 and elevated concentrations of *Asterionella formosa* characterize diatom assemblages since ~1980 CE (Ekdahl et al., 2004; Gushulak et al., 2022; Figures 1 and 17). Analysis at annual scale from 1930 to 1980 CE confirmed the near disappearance of *Lindavia michiganiana* after 1950 CE as well as the increase in the chrysophyte genus *Synura* in the mid-1950s (Marshall et al., 2023). The higher-resolution analysis refined the pattern of subsequent increases in the planktonic diatoms *Cyclotella distinguenda*, *Lindavia intermedia*, and *Fragilaria andreseniana* (identified as *Fragilaria tenera* var. *nanana* in Gushulak et al., 2022), replacing non-planktonic taxa (e.g. *Achnanthyidium* spp.; Figure 16) through the 1950–1970s (Marshall et al., 2023).

Discussion

The rapid rise in ²³⁹⁺²⁴⁰Pu between ~1948 and 1964 CE (Figures 11b and 17) based on the Crawford Lake varve age model (Supplemental Table S1, Figure S9) compares well with the global record (United Nations Scientific Committee on the Effects of Atomic Radiation (UNSCEAR), 2000). Atmospheric fallout from above-ground nuclear tests is also recorded by the overprint of the ~1100–1200-year “old carbon error” beginning in the early 1950s, despite potential incomplete treatment for dolomite in samples from core CL-2011 (Figures 11a, 18 and Table 2). The annually resolved varved succession at Crawford Lake arises from inhibited bioturbation of the lakebed, caused by elevated salinities, not anoxia, within the monimolimnion (Heyde, 2021; Llew-Williams, 2022). The oxygenated monimolimnion minimizes mobilization of ²³⁹Pu (Francis, 2007), allowing this proposed primary stratigraphic marker for the base of the Anthropocene to be preserved with outstanding fidelity at Crawford Lake. These varved deposits have also preserved an annually resolved record of the Great Acceleration. The global increase in fossil fuel combustion during the 1950s is recorded by a sharp increase in the concentration of SCPs, including particles smaller than 10 μm in freeze core CRA22-2FT-B2, and depleted δ¹⁵N values (Figures 12, 13, and 17). The similar increase in SCPs in “pollen slides” allows the early 1950s to be easily identified in cores across the basin, including gravity core CL-19 (Figure 19) where varve couplet precision was not possible. This, and a well-dated pollen zonation to identify this boundary that coincides with the regional decline in elm pollen due to Dutch elm disease, allows independent calibration of the ²¹⁰Pb age model, supported by the peak in ¹³⁷Cs activity (Figure 9).

Although the karstic basin is well-buffered, the limnology of Crawford Lake was affected by the influx of particulate carbon through atmospheric deposition, as well as acidic precipitation. Reduced calcite precipitation during the 1950s and 60s is recorded by very thin light-colored laminae in dark bands punctuated by a triplet of prominent laminae marking the summers of 1956, 1957, and 1958 CE (Supplemental Figure S9) that allow easy correlation between freeze cores across the deep basin of Crawford Lake (Figures 5–8). Micro-XRF analysis of freeze core CL-2011 identified high concentrations of terrigenous elements in these calcium-poor sediments around the proposed base of the Anthropocene (Figures 14 and 18). The biotic response to these stressors in the 1940–1970s is evident in the similarity of the siliceous microfossil record to SCP and δ¹⁵N profiles (Figure 17), notably an increase in non-planktonic diatom concentrations and chrysophyte assemblages dominated by the colonial genera *Synura* and *Dinobryon* (Figures 16 and 17). Changes

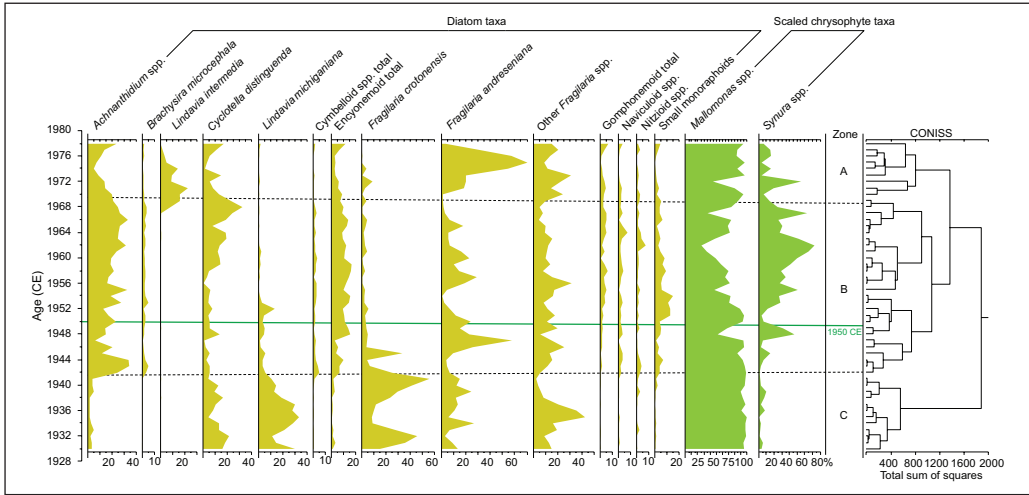


Figure 16. Summary of analysis of siliceous microfossils at annual resolution from core CRA19-2FT-D1. Stratigraphically constrained cluster analysis identified three zones, with Zone B defined by a decline in the planktonic diatoms *Lindavia michiganiana* and *Fragilaria crotonensis* that dominated Zone C and sharp increases in non-planktonic taxa such as *Achnanthydium* spp. Significant dissimilarity was also noted around 1950 CE (solid line), primarily in the scaled chrysophyte record, with several species of *Synura* dominating assemblages in the upper part of zone B. Modified from Marshall et al. (2023). Reproduced in color in online version.

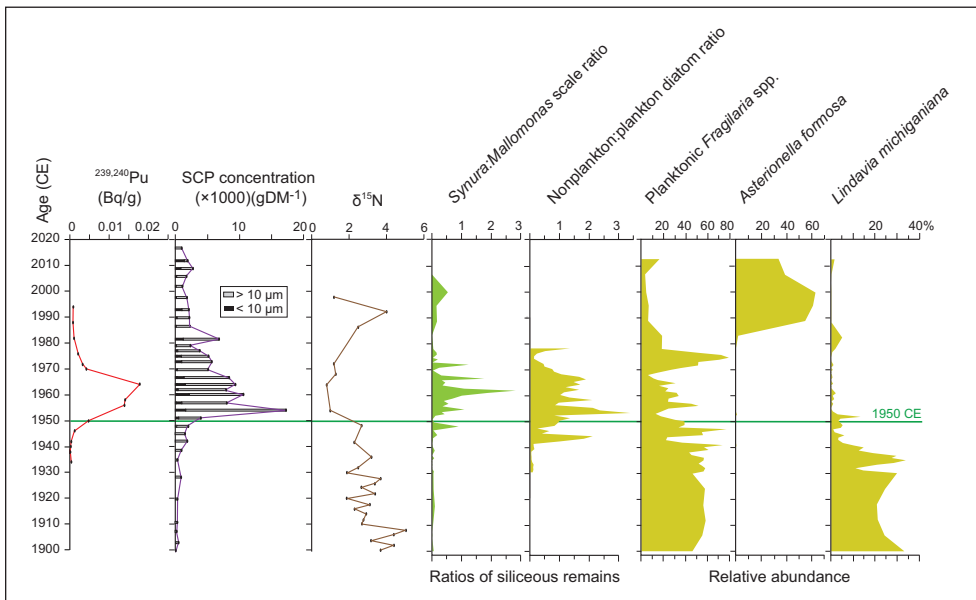


Figure 17. Summary of key Anthropocene markers and the synchronous ecosystem response recorded by siliceous microfossils around 1950 CE in varve-age dated samples from freeze cores from the deep basin of Crawford Lake. Abundant SCPs and depleted $\delta^{15}\text{N}$ values record increased fossil fuel combustion following the Second World War, when plutonium fallout first appears in varved sediment. The increase in non-planktonic diatoms and the scaled chrysophyte genus *Synura* across the proposed Anthropocene GSSP (marked by horizontal line) begins in the 1940s and declines through the 1970s, as do the physical Anthropocene markers. Reproduced in color in online version.

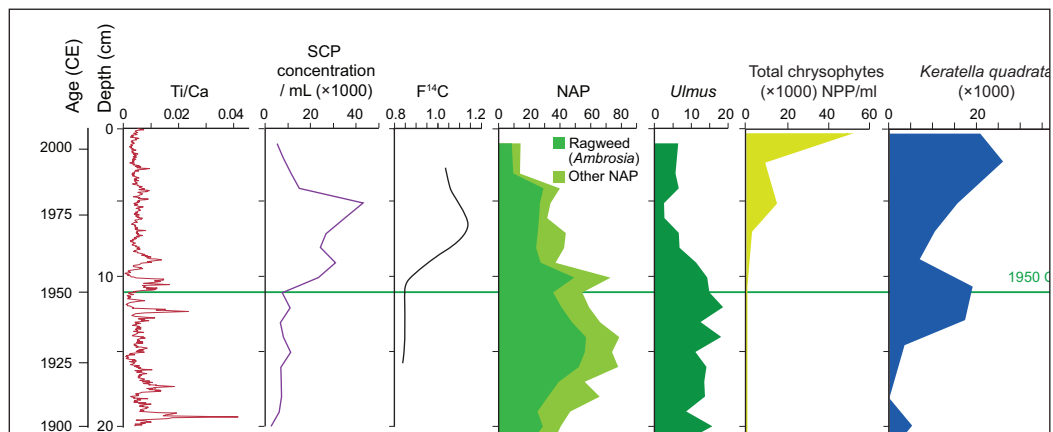


Figure 18. Summary of key Anthropocene markers in freeze core CL-2011. The proposed base of the Anthropocene (1950 CE, shown by horizontal line) is marked by high XRF activity attributed to terrigenous elements (e.g., titanium) in calcite-poor sediments and a sharp increase in concentration of SCPs in palynological preparations. The radiocarbon 'bomb pulse' coincides with the sharp decline in *Ulmus* pollen resulting from Dutch elm disease. Reforestation also helps identify the late 20th century, as do several non-pollen palynomorphs, such as loricae of the chrysophyte *Dinobryon divergens* and the rotifer *Keratella quadrata*, almost unknown from earlier sediments from Crawford Lake. Reproduced in color in online version.

at the base of the food chain, including a decline in overall primary production in surface waters recorded by fossil pigments relative to the early 20th century (Figure 15), are reflected by changes in consumers, notably a sharp decrease in the cladoceran genus *Bosmina* and the rotifer *Keratella cochlearis*. Loricae of the rotifer *Keratella quadrata* and of the colonial chrysophyte *Dinobryon divergens* characterize the Anthropocene, as here proposed, in palynological preparations from Crawford Lake (Figures 18 and 19).

The subsequent decline in SCP concentrations in core CRA19-2FT-B2 (Figures 12 and 17) and in palynological preparations from cores CL-2011 and CL-19 (Figures 18 and 19) appears to correspond to more strict environmental regulations beginning in the 1970s. Emission controls were adopted at steel mills operating in the industrial city of Hamilton ~30 km to the SSE, and the last open-hearth furnace at Stelco closed in 1984 CE (<https://www.thespec.com/news/hamilton-region/2012/02/11/hamilton-s-steel-industry-from-birth-to-boom-and-beyond.html>). Dofasco had abandoned open-hearth technologies in 1954 CE (Supplemental Figure S2), and the decline in SCP concentrations after the peak measured that year can probably be attributed to this change. The regional decline in high-temperature coal combustion may have contributed to the return to slightly enriched $\delta^{15}\text{N}$ values measured in varves from the late 1980s and early 90s, but the return to depleted values in the most recent sample analyzed suggests that this protected site may have become impacted by global stressors. The dominance of *Asterionella formosa* since 1980 CE (Figures 1 and 17) defines a major diatom assemblage change that resembles environments during the Medieval Warm Period (Ekdahl et al., 2004). This may suggest a response to a warmer climate, by comparison with changes in chrysophyte assemblages, as discussed in Gushulak et al. (2022). This is consistent with evidence of a slight increase in primary producers in surface waters of Crawford Lake following mid-20th century lows, recorded by algal palynomorph assemblages and fossil pigments and thicker/ more prominent calcite laminae (Figures 15–19).

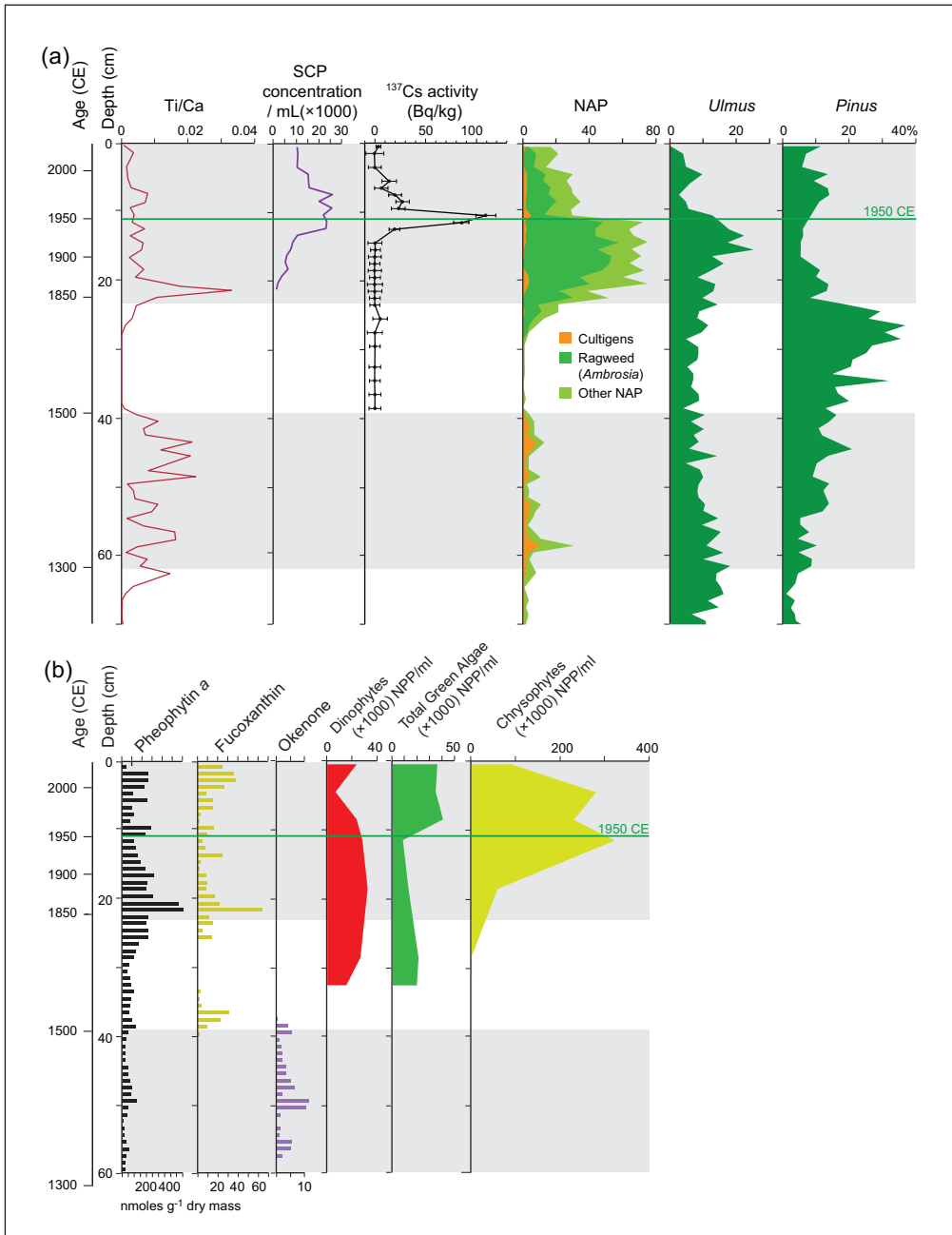


Figure 19. Summary of key Anthropocene markers plotted against depth in gravity core CL-19. a) Increases in terrigenous elements and non-arboreal pollen (NAP) identify two distinct intervals of human impact on Crawford Lake, highlighted by stippling. The decline in elm pollen (*Ulmus*) and increase in ^{137}Cs activity identify the mid-20th century, when increased fossil fuel combustion produced a sharp increase in SCP concentration in palynological preparations. b) Fossil pigments and algal palynomorphs record an increase in green algae and the chrysophyte *Dinobryon divergens* since the mid-20th century, recording a slight increase in overall primary productivity. The absence of the fossil pigment okenone confirms the well-oxygenated water column in this unusual meromictic lake since the early 16th century. Reproduced in color in online version.

We propose placing the GSSP for the Anthropocene series/epoch at the base of the calcite lamina deposited in the summer of 1950 CE in freeze core CRA22-1FR-3 (Figure 7), based on the rapid increase in key Anthropocene markers between ~1948 CE and 1954 CE (Figure 17). Because the varve chronology allows confident correlation across the deep basin of Crawford Lake at sub-annual scale, geochemical evidence of acid precipitation on the catchment in a freeze core collected in 2011 (Core CL-2011; Figure 14) can be related to the high influx of SCPs in core CRA19-2FT-B2 that was imaged at ultrahigh resolution to develop the varve chronology (Figure 6) and to the biotic responses to these stressors presented in this article (Figures 15–19) and in published studies (Ekdahl et al., 2004, 2007; Rybak and Dickman, 1988; Rybak et al., 1987). The Great Acceleration (Head et al., 2022; Steffen et al., 2015) is amplified by industrial emissions from the city of Hamilton where the steel industry boomed between the 1940s and 1980s, a proxy for industrialization across northeastern North America. Biotic proxies in the varved sediment also record a response to global stressors, particularly since 1969 CE, when the lake became protected by Conservation Halton.

Whereas earlier studies assumed that bottom waters were anoxic below the permanent chemocline, instrumental measurements over a 3-year period identified well-oxygenated conditions in the monimolimnion (Figure 3 and Supplemental Figure S4), with mean DO = 8.2 mg/L (range 4.6–11.4 mg/L, $n=78$) comparable to values measured in aquifers transecting the karstic basin (Llew-Williams, 2022). Metabolically active omnivores and detritivores reported from below the chemocline of Crawford Lake (Heyde, 2021; Mazumder, 1983) support the instrumental record, as does the absence of pigments of obligately anaerobic bacteria that were present through the 15th century (Figure 15). The highly unusual non-reducing bottom waters in this meromictic lake, from which benthic organisms larger than microscopic groundwater-dwelling ostracods were excluded by the higher salinity and alkalinity (Figure 3 and Supplemental Figure S5), hinder the mobilization of plutonium (Francis, 2007). The excellent comparison between profiles of $^{239+240}\text{Pu}$ and $^{240/239}\text{Pu}$ and the global record of nuclear and thermonuclear testing (Figure 11b) illustrates the stability of this element, proposed as the best primary marker for the Anthropocene with a base in the mid-20th century (Zalasiewicz et al., 2017).

The GSSP has a depth of 15.6 cm in core CRA22-1FR-3 (Figure 7) which is archived at the National Biodiversity Cryobank of Canada (Canadian Museum of Nature, Ottawa). This core was analyzed for ^{239}Pu , SCPs and gamma radiation, as well as radiocarbon analysis of the gamma samples following their non-destructive analysis (Supplemental Table S17–S20; Supplemental Figures S27–31). Analysis of polychlorinated biphenyls (PCBs) from ~1876 to 2007 in this core did not reveal concentrations above background through the 20th century (Supplemental Table S14), suggesting that the small Crawford Lake in a small catchment in rural Ontario is not a useful repository for the local deposition of persistent organic pollutants (POPs).

The proposed GSSP level is dated by varve chronology to 1950, placed at the base of the second very thin calcite layer in the lowermost of two dark bands of sediment deposited across Crawford Lake in response to acid precipitation (Figure 7; also see Figures 5, 6 and Supplemental Figures S7 and S9). The GSSP horizon aligns closely with the initial phase of a sharp rise in $^{239+240}\text{Pu}$ (Figure 11b); the peak in ^{137}Cs (Figure 9); a sharp decline in nonarborescent and elm pollen, the latter a regional marker of Dutch elm disease (Figures 10 and 18a); the initial sharp rise in SCP concentrations (Figure 12); a reduction in $\delta^{15}\text{N}$ values (Figure 13); rises in the elemental concentrations of Fe, K, Ti, Cu, and Pb, and a decline in Ca (Figure 14); and rises in the chlorophyll *a*:pheophytin *a* ratio (Figure 15). These stratigraphic indicators together facilitate correlation to the proposed GSSP locally with seasonal to annual precision, and globally within a few years. An Anthropocene GSSP dated 1950 CE has the following advantages. (1) 1950 is a round number

and by convention is the “present” in BP (before present) as determined by radiocarbon dating and so a natural marker for the Quaternary community; (2) it is also the year widely used within the Earth System community from where the term Anthropocene originated; (3) although ^{239}Pu is clearly tied to the nuclear age, the year 1950 might be less troubling to those concerned with a link between the Anthropocene and thermonuclear weapons testing which began later (in 1952) or the bombing of Japan in 1945 CE.

The name “Crawfordian” is proposed for the associated stage and age, with reference to the name of the type locality following Salvador (1994). Earlier impacts, notably those resulting from Indigenous agriculture between the late 13th and latest 15th centuries and logging of the catchment beginning in the mid-19th century, are recorded by numerous proxies occurring tens of centimeters below the proposed GSSP. This illustrates the difference between diachronous local to regional human impacts and the rapidity and magnitude of change in the Earth System chosen to characterize the Anthropocene as a series/epoch in a supermajority vote by the AWG in May 2019 (Waters et al., 2023). The Interpretive Center at the Crawford Lake Conservation Area, which is a short walk from the proposed type locality, the Canadian Museum of Nature (CMN) in Ottawa where the proposed GSSP core is curated, and the Royal Ontario Museum in Toronto which will house the proposed parastratotype, would together allow effective communication of this distinction to a broad audience.

Acknowledgements

We are pleased to acknowledge the Haus der Kulturen der Welt (HKW), Berlin for collaborating with the Anthropocene Working Group in the assessment of the candidate GSSP sites. The collaboration was realized in the framework of HKW’s long-term initiative Anthropocene Curriculum, an international project for experimental forms of Anthropocene research and education developed by HKW and the Max Planck Institute for the History of Science (MPIWG, Berlin) since 2013. We acknowledge additional funding from NSERC Discovery grants to F.M.G. McCarthy, R.T. Patterson, M.J. Head, B.F. Cumming, M.F.J. Pisaric, P.R. Leavitt, and J.I. Boyce. Several other institutions have provided in-kind or financial support, including Conservation Halton, Brock University, Carleton University, the Canadian Museum of Nature and the Royal Ontario Museum. In addition to those whose contributions are mentioned in this paper, the authors are grateful to all members of Team Crawford, notably S. Turner (UCL), B. Bartley and B. O’Reilly (Conservation Halton), S. Alderson, U. Brand, A. Krueger, and M. Lozon (Brock University), M. MacKinnon (OSPM Solutions), D. Bateson (U. Regina), G. Tyrrell (U. Leicester), D. Metsger and S. Brothers (ROM), S. Murseli (U Ottawa), E. Reinhardt (McMaster U), W. Finlayson (Wilfred Laurier U.), Charlie Turton (U. Toronto), Wyandot Elder C. Tammaro and videographers J. Rosen (Fleming College/ROM), J. Head (Brock U.) and N. de Pencier and the rest of the Mercury Films crew. Samples and data that form the basis of this study were collected from land covered by Canada’s Upper Canada Treaties, the traditional territory of Anishinaabeg, Wendat, Haudenosaunee, and Ojibway/Chippewa First Nations peoples. We are grateful to Associate Editor S. Turner and two anonymous reviewers whose insights contributed to the final draft of this paper.

Declaration of conflicting interests

The author(s) declared no potential conflicts of interest with respect to the research, authorship, and/or publication of this article.

Funding

The author(s) disclosed receipt of the following financial support for the research, authorship, and/or publication of this article: The Haus der Kulturen der Welt for analysis of key Anthropocene markers for this article. We also acknowledge additional funding from NSERC Discovery grants to F.M.G. McCarthy, R.T. Patterson, M.J. Head, B.F. Cumming, M.F.J. Pisaric, P.R. Leavitt, and J.I. Boyce. Several other institutions

have provided financial support, including Brock University, Carleton University, the Canadian Museum of Nature, Conservation Halton, and the Royal Ontario Museum.

ORCID iDs

Francine MG McCarthy  <https://orcid.org/0000-0001-5038-8355>

A. Cale Gushulak  <https://orcid.org/0000-0001-9780-3886>

Peter R Leavitt  <https://orcid.org/0000-0001-9805-9307>

Irka Hajdas  <https://orcid.org/0000-0003-2373-2725>

Supplemental material

Supplemental material for this article is available online.

References

- Appleby PG and Oldfield F (1978) The calculation of lead-210 dates assuming a constant rate of supply of unsupported ^{210}Pb to the sediment. *CATENA* 5(1): 1–8.
- Battarbee RW, Jones VJ, Flower RJ, et al. (2001) Diatoms. In: Smol JP, Birks HJB and Last WM (eds) *Tracking Environmental Change Using Lake Sediments, Vol. 3: Terrestrial, Algal, and Siliceous Indicators*. Dordrecht: Kluwer Academic Publishers, pp.55–202.
- Boyko-Diakonow M (1979) The laminated sediments of Crawford Lake, southern Ontario, Canada. In: Schluchter C (ed.) *Moraines and Varves*. Rotterdam: A. A. Balkema, pp.303–307.
- Boyko M (1973) *European impact on the vegetation around Crawford Lake in Southern Ontario*. MSc Thesis, University of Toronto.
- Byrne R and Finlayson WD (1998) Iroquoian agriculture and forest clearance at Crawford Lake, Ontario. In: Finlayson WD (ed.) *Iroquoian Peoples of the Land of Rocks and Water A.D. 1000–1650: A Study in Settlement Archaeology*. London: Museum of Archaeology, London, Ontario, Canada: The University of Western Ontario, Special Publication 1, pp.94–107.
- Cranm CA, Murseli S, St-Jean G, et al. (2017) First status report on radiocarbon sample preparation techniques at the A.E. Lalonde AMS Laboratory (Ottawa, Canada). *Radiocarbon* 59(3): 695–704.
- Dickman M (1985) Seasonal succession and microlamina formation in a meromictic lake displaying varved sediments. *Sedimentology* 32: 109–118.
- Dickman MD (1979) A possible varving mechanism for meromictic lakes. *Quaternary Research* 11: 113–124.
- Ekdahl EJ, Teranes JL, Guilderson TP, et al. (2004) Prehistorical record of cultural eutrophication from Crawford Lake, Canada. *Geology* 32: 745–748.
- Ekdahl EJ, Teranes JL, Wittkop CA, et al. (2007) Diatom assemblage response to Iroquoian and Euro-Canadian eutrophication of Crawford Lake, Ontario, Canada. *Journal of Paleolimnology* 37: 233–246.
- Finlayson WD (1998) *Iroquoian Peoples of the Land of Rocks and Water A.D. 1000 to 1650: A Study in Settlement Archaeology*. London Museum of Archaeology London, Ontario, Canada: The University of Western Ontario, Special Publication 1, p.506
- Finlayson WD, Byrne AR and McAndrews JA (1973) Iroquoian settlement and subsistence patterns near Crawford Lake, Ontario. *Bulletin (Canadian Archaeological Association)* 5: 134–136.
- Francis AJ (2007) Microbial mobilization and immobilization of plutonium. *Journal of Alloys and Compounds* 444–445: 500–505.
- Gregory BRB, Patterson RT, Reinhardt EG, et al. (2019) An evaluation of methodologies for calibrating Itrax X-ray fluorescence counts with ICP-MS concentration data for discrete sediment samples. *Chemical Geology* 521: 12–27.
- Gregory BRB, Reinhardt EG, Macumber AL, et al. (2017) Sequential sample reservoirs for Itrax-XRF analysis of discrete samples. *Journal of Paleolimnology* 57(3): 287–293.
- Gushulak CA, Marshall M, Cumming BF, et al. (2022) Siliceous algae response to the ‘Great Acceleration’ of the mid-20th century in Crawford Lake (Ontario, Canada): A potential candidate for the anthropocene GSSP. *The Anthropocene Review* 9: 571–590.

- Hajdas I, Ascough P, Garnett MH, et al. (2021) Radiocarbon dating. *Nature Reviews Methods Primers* 1: 62.
- Han X and Dickman M (1995) Changes in ^{13}C content of the organic component of lake sediments during the last 500 years in Crawford Lake, South Ontario, Canada. *Hydrobiologia* 310: 177–187.
- Head MJ, Steffen W, Fagerlind D, et al. (2022) The Great Acceleration is real and provides a quantitative basis for the proposed anthropocene Series/Epoch. *Episodes* 45: 359–376.
- Heyde A (2021) *Crawford lake consumers: Water column and palynological studies*. MSc Thesis, Brock University.
- Hua Q, Turnbull JC, Santos GM, et al. (2022) Atmospheric radiocarbon for the period 1950–2019. *Radiocarbon* 64(4): 723–745.
- Hutchinson GE (1957) *A Treatise on Limnology. Vol. I: Geography, Physics, and Chemistry*. New York, NY: Wiley.
- Karrow PF (1987) Quaternary geology of the Hamilton Cambridge area, Southern Ontario. *Ontario Geological Survey Report* 255: 94.
- Krueger AM (2012) *Freshwater dinoflagellates as proxies of cultural eutrophication: a case study from Crawford Lake, Ontario*. MSc Thesis, Brock University.
- Krueger AM and McCarthy FMG (2016) Great Canadian *Lagerstätten* 5. Crawford Lake – A Canadian Holocene lacustrine *Konservat-Lagerstätte* with two-century-old viable dinoflagellate cysts. *Geoscience Canada* 43: 123–132.
- Lafond K, Walsh CR, Patterson RT, et al. (2022) Influence of climatic trends and cycles on the annual varve deposition in Crawford Lake, Ontario, Canada. 2022. Session FS6 – Varves records: from tracking natural and anthropogenically induced changes of the environment and climate to improving chronologies of past events, Nov. 30. International Association of Limnogeology and International Paleolimnology Association 2022 Joint Meeting. 27 November – 1 December, 2022.
- Lan Y and Breslin VT (1999) Sedimentary records of spheroidal carbonaceous particles from fossil-fuel combustion in western Lake Ontario. *Journal of Great Lakes Research* 25(3): 443–454.
- Leavitt PR and Hodgson DA (2001) Sedimentary pigments. In: Smol JP, Birks HJB and Last WM (eds) *Tracking Environmental Change Using Lake Sediments. Volume 3: Terrestrial, Algal and Siliceous Indicators*. Dordrecht, Netherlands: Kluwer, pp.295–325.
- Llew-Williams B (2022) *The hydrological and limnological characterization of two Canadian water catchments sensitive to anthropogenic influences: Crawford Lake, Ontario and Old Crow Flats, Yukon*. MSc Thesis, Brock University.
- Llew-Williams BM, McCarthy FMG, Krueger AM, et al. (in revision) Varve formation in meromictic Crawford Lake, Ontario, Canada: Important process for characterizing the Anthropocene epoch. In revision to *Journal of Paleolimnology*
- Lokas E, Wachniew P, Baccolo G, et al. (2022) Unveiling the extreme environmental radioactivity of cryoconite from a Norwegian glacier. *The Science of the Total Environment* 814: 152656.
- Marshall M (2021) *Annual-scale (1930–1990) assessment of anthropogenic influences on the assemblage structure of Golden-Brown Algae (Chrysophytes) in Crawford Lake, Ontario, Canada*. MSc Thesis, Carleton University.
- Marshall MG, Hamilton PB, Lafond KM, et al. (2023) Annual-scale assessment of mid-20th century anthropogenic impacts on the algal ecology of Crawford Lake, Ontario, Canada. *PeerJ* 11: e14847.
- Mazumder A (1983) *Ecological interactions between zooplankton and photosynthetic bacteria in Crawford Lake, Ontario*. MSc Thesis, Brock University.
- McAndrews JH (1994) Pollen diagrams for southern Ontario applied to archaeology. In: MacDonald R (ed.) *Great Lakes Archaeology and Paleoeology: Exploring Interdisciplinary Initiatives for the Nineties*. Waterloo, Ontario, Canada: Quaternary Sciences Institute, University of Waterloo, pp.179–196.
- McAndrews JH, Berti AA and Norris G (1973) *Key to the Quaternary Pollen and Spores of the Great Lakes Region*. Toronto, Ontario, Canada: ROM Miscellaneous Publication.
- McAndrews JH and Boyko-Diakonow M (1989) Pollen analysis of varved sediment at Crawford Lake, Ontario: Evidence of Indian and European farming. In: Fulton RJ (ed.) *Quaternary Geology of Canada and Greenland, Geology of Canada*, vol. 1. Ottawa, Ontario, Canada: Geological Survey of Canada, pp.528–530

- McAndrews JH and Turton CL (2007) Canada geese dispersed cultigen pollen grains from prehistoric Iroquoian fields to Crawford Lake, Ontario, Canada. *Palynology* 31: 9–18.
- McAndrews JH and Turton CL (2010) Fungal spores record Iroquoian and Canadian agriculture in 2nd millennium AD sediment of Crawford Lake, Ontario, Canada. *Vegetation History and Archaeobotany* 19: 495–501.
- McCarthy FMG (2022) Chapter 9. Stratigraphy: finding global markers in a small Canadian lake. In: Thomas JA (ed.) *Altered Earth: Getting the Anthropocene Right*. Cambridge: Cambridge University Press, pp.196–208.
- McCarthy FMG, Pilkington PM, Volik O, et al. (2021) Non-pollen palynomorphs in freshwater sediments and their paleolimnological potential. In: Marret F, O’Keefe J, Sterloff O, et al (eds) *TMS Special Publication SP511, Applications of Non-pollen Palynomorphs from Palaeoenvironmental Reconstructions to Biostratigraphy*. London: Geological Society of London, pp.121–150.
- Moraal JM, McCarthy FMG, Rose NL, et al. (in prep.) Spheroidal carbonaceous particles and other black carbon in palynological preparations as proxies of anthropogenic impact in Crawford Lake, Ontario, Canada. For submission to *Palynology*.
- Priebe EH (2019) *Investigating new approaches for mapping groundwater systems in karstic carbonate bedrock: A case study in the Early Silurian formations of the Niagara Escarpment cuesta, southern Ontario, Canada*. PhD Thesis, University of Waterloo.
- Reimer PJ, Austin WEN, Bard E, et al. (2020) The IntCal20 Northern Hemisphere radiocarbon age calibration curve (0–55 cal kBP). *Radiocarbon* 62(4): 725–757.
- Rakowski AZ, Nadeau M-J, Nakamura T, et al. (2013) Radiocarbon method in environmental monitoring of CO₂ emission. *Nuclear Instruments and Methods in Physics Research B* 294: 503–507
- Rose NL (1994) A note on further refinements to a procedure for the extraction of carbonaceous fly-ash particles from sediments. *Journal of Paleolimnology* 11: 201–204.
- Rose NL (2008) Quality control in the analysis of lake sediments for spheroidal carbonaceous particles. *Limnology and Oceanography Methods* 6: 172–179.
- Rose NL (2015) Spheroidal carbonaceous fly ash particles provide a globally synchronous stratigraphic marker for the Anthropocene. *Environmental Science & Technology* 49(7): 4155–4162.
- Rothwell RG and Croudace IW (2015) Micro-XRF studies of sediment cores: A perspective on capability and application in environmental sciences. In: Croudace IW and Rothwell RG (eds) *Micro-XRF Studies of Sediment Cores, Developments in Paleoenvironmental Research*, vol. 17, Dordrecht, Netherlands: Springer. pp.1–21.
- Ruff M, Szidat S, Gaggeler HW, et al. (2010) Gaseous radiocarbon measurements of small samples. *Nuclear Instruments and Methods in Physics Research Section B: Beam Interactions with Materials and Atoms* 268: 790–794.
- Rybak M and Dickman M (1988) Paleocological reconstruction of changes in the productivity of a small, meromictic lake in Southern Ontario, Canada. *Hydrobiologia* 169: 293–306.
- Rybak M, Rybak I and Dickman M (1987) Fossil chrysophycean cyst flora in a small meromictic lake in southern Ontario, and its paleoecological interpretation. *Canadian Journal of Botany* 65: 2425–2440.
- Salvador A (Ed.) (1994) *International Stratigraphic Guide: A Guide to Stratigraphic Classification, Terminology, and Procedure*, 2nd edition. Boulder, Colorado: International Subcommission on Stratigraphic Classification of IUGS International Commission on Stratigraphy and The Geological Society of America.
- Steffen W, Broadgate W, Deutsch L, et al. (2015) The trajectory of the Anthropocene: The Great Acceleration. *The Anthropocene Review* 2(1): 81–98.
- Stuiver M and Polach HA (1977) Discussion: Reporting of ¹⁴C data. *Radiocarbon* 19(3): 355–363.
- Synal HA, Stocker M and Suter M (2007) MICADAS: A new compact radiocarbon AMS system. *Nuclear Instruments and Methods in Physics Research Section B-Beam Interactions with Materials and Atoms* 259: 7–13
- Syvitski J, Waters CN, Day J, et al. (2020) Extraordinary human energy consumption and resultant geological impacts beginning around 1950 CE initiated the proposed Anthropocene Epoch. *Communications Earth & Environment* 1: 32.
- Turton CL and McAndrews JH (2006) Rotifer loricas in second millennium sediment of Crawford Lake, Ontario, Canada. *Review of Palaeobotany and Palynology* 141: 1–6.

- United Nations Scientific Committee on the Effects of Atomic Radiation (UNSCEAR) (2000) Sources and Effects of Ionizing Radiation. *Report, Volume 1*. UNSCEAR 2020/2021.
- Waters CN, Turner SD, Zalasiewicz J, et al. (2023) Candidate sites and other reference sections for the Global boundary Stratotype Section and Point (GSSP) of the Anthropocene series. *The Anthropocene Review* 10(1): 3–24 (in this issue).
- Wong C, Ballegooyen K, Ignace L, et al. (2020) Towards reconciliation: 10 calls to action to natural scientists working in Canada. *Facets* 5(1): 769–783.
- Wu F, Zheng J, Liao H, et al. (2011) Anomalous plutonium isotopic ratios in sediments of Lake Qinghai from the Qinghai-Tibetan Plateau, China. *Environmental Science & Technology* 45: 9188–9194.
- Zalasiewicz J, Waters CN, Summerhayes CP, et al. (2017) The Working Group on the Anthropocene: Summary of evidence and interim recommendations. *Anthropocene* 19: 55–60.